Master Thesis in Reservoir Physics

Enhanced Oil Recovery by CO_2 and CO_2-Foam in Fractured Carbonates

Tom Ydstebø

Department of Physics and Technology

University of Bergen

June 2013

Summary

This thesis is a part of an ongoing study of integrated enhanced oil recovery methods in the Reservoir Physics research group at the Department of Physics and Technology at the University of Bergen. The aim of this thesis has been to study liquid CO_2 and liquid CO_2-foam injection in whole and fractured Edward limestone cores.

Routine core analysis, such as porosity and permeability measurements, was performed on 50 cores. Seven limestone core plugs were aged in crude oil to alter the originally strongly water-wet wettability preference to oil-wet.

Two laboratory systems were designed a part of this thesis to perform CO_2 injection tests at elevated pressures for 1) pure CO_2 injection and 2) CO_2-foam injection. The line pressure on both the experimental systems was 95 bars. A total of 19 successful CO_2 injection experiments were performed at elevated pressures to develop miscibility between the injected CO_2 and oil in the pore space.

Sixteen pure CO_2 injection tests were performed with variations in wettability, presence of a fracture and an initial water phase were investigated. Final recovery range between 59-100%OOIP for all CO_2 injections. The final recovery was somewhat higher for whole cores compared to fractured core plugs, but the fracture significantly reduced the oil production rate. A slight effect from wettability could be observed, but was not significant. The presence of water in the pore space reduced the oil production rate, especially in fractured cores. This was explained by a reduction in the effective diffusion rate between oil and CO_2.

The injection of CO_2-foam significantly increased the rate of production, but not the final oil recovery, compared to pure CO_2 injection in fractured cores with a production above 90%OOIP.

Two of the experimental results were further investigated in a numerical model using CMG (Computer Modeling Group) software. The numerical model successfully reproduced the experimental results and investigated parameters such as the flow properties, diffusion coefficient and wettability preference.

Acknowledgements

First I would like to thank my supervisors Prof. Arne Graue and Dr. Martin Fernø at the Department of Physics and Technology at the University of Bergen for their guidance and for giving me the opportunity to travel to College Station Texas to do research.

I would also like to thank Dr. Åsmund Haugen, Dr. Geir Ersland, MSc Øyvind Eide and Inez Buzdugan for useful advices and help with the experimental work.

Thanks to Prof. David Schechter for inviting students to Texas A&M in College State and giving us the opportunity to do research in their lab. Many thanks to Fransisco Tovar for his professional expertise and for helping with the CO_2-foam experiments.

I would also like to thank my fellow students both during the bachelor and master studies for many interesting discussions and social events, and especially Stig Langlo for being an excellent team player during our cooperation in the lab and studies.

I thank my parents (Kari and Bjarte) and two siblings (Kristian and Renate) for their support and motivations during my 5 years of studying at the University of Bergen.

Bergen, May 2013
Tom Ydstebø

Contents

Introduction

A great amount of oil, over 50% in most cases, is left behind in the reservoir after conventional primary and secondary oil recovery processes. This unrecovered oil may be produced with a tertiary enhanced oil recovery process and thereby increase our petroleum energy source for years to come. This has led to an increased interest in enhanced oil recovery (EOR) processes due to the global need of oil supply and high oil prices.

The purpose of EOR is to increase the macroscopic sweep efficiency and to enhance the microscopic displacement efficiency in the reservoir compared to conventional recovery processes such as water injection. In heterogeneous reservoirs, recoverable oil is increased by reducing the flow in high permeable zones or increasing the viscosity of the injected fluids to increase the macroscopic sweep. This can be achieved by foam or polymer injection. The microscopic displacement efficiency can be increased by reducing the interfacial tension and thereby reduce the residual oil saturation in the reservoir pores. Surfactants and miscible flooding are examples of such displacement.

It is documented that almost half of the world oil reserves is located in carbonate reservoirs, which are characterized by a large degree of heterogeneities including fractures with large permeability differences between matrix and fractures. The carbonate reservoirs have also often neutral and oil wetting preferences leading to a recovery of less than 30% OOIP(Hognesen et al., 2005).

The increased atmospheric CO_2 concentration and its effect on the climate change are currently of great focus around the world, in addition to the need for additional energy needs for the future. Using CO_2 for EOR could contribute to decrease the CO_2 emissions and thereby reduce the greenhouse effect, combined with additional available energy for the future. This process is called CCUS (carbon capture utilization and storage) and may play a vital role worldwide(IEA, 2013).

There have been several CO_2 EOR projects onshore in the world. During a miscible displacement of oil by CO_2, all the oil could theoretically be produced by reducing the residual oil. CO_2 injection into mature fields has proven to be an effective method for enhanced oil recovery. The low viscosity of the injected CO_2 at reservoir conditions leads the poor macroscopic sweep, especially in heterogeneous reservoirs.

Foam injection increase the displacement efficiency compared to gas injection in heterogeneous and fractured reservoir (Rossen, 1996). Foam generates when gas contacts surfactant in reservoir by co-injecting gas and surfactant or by alternating surfactant and gas.

Foam is used to 1) increase the gas viscosity, 2) blocking the high permeable swept zones and divert the fluid into upswept zones and 3) reduce the gas-oil ratio (GOR).

This thesis consists of 10 chapters. Chapter 1 gives an introduction to fundamental principles relevant for this thesis. Chapter 2 and 3 provides an overview of CO_2 properties and the fundamentals behind foam generation and flow capacities. The experimental procedures and designs are provided in chapter 4 and 5. The experimental results are presented in chapter 6. Discussions of the work are given in chapter 7 and the general conclusions in chapter 8. Chapter 9 and 10 gives the nomenclature and references used in the thesis.

1 Fundamental Reservoir Physics

This chapter gives a theoretical introduction to fundamental principles within reservoir physics. The procedures to measure the parameters are described in section 4.

1.1 Porosity

Porosity is the parameters that define the fluid-storage capacity of a rock, which are the pores. It is the part of the rock that is not occupied with rock grains and mineral cement and is divided into absolute and effective porosity. Absolute porosity is defined as the ratio between the total pore volume V_{pa} and the bulk volume V_b of the rock.

$$\Phi_a = \frac{V_{pa}}{V_b} \tag{1}$$

Effective porosity is the ratio between the total volume of interconnected pores V_p and the bulk volume V_b.

$$\Phi = \frac{V_p}{V_b} \tag{2}$$

When mentioning porosity in reservoir engineering, it is usually referred to effective porosity. This is because the interconnected pores conduct the mobile hydrocarbons.

1.2 Fluid saturation

Fluid saturation describes the fraction of the pore volume that is occupied by a particular fluid. Since the pores can be filled with water, oil and gas, the pore content can be written as:

$$\mathrm{V}_p = \mathrm{V}_w + \mathrm{V}_o + \mathrm{V}_g \tag{3}$$

Where V_p is the pore volume and V_w, V_o and V_g are the volumes of water, oil and gas, respectively. This leads to the definition of saturation, S, as a fraction of the pore volume occupied by a particular fluid:

$$S_i \stackrel{\text{def}}{=} \frac{V_i}{V_p}, i = 1, \dots, n \tag{4}$$

Where n denotes the total number of fluid phase present in the porous medium (Zolotukhin, 2000), which leads to:

$$\sum_{i=1}^{n} S_i = 1 \tag{5}$$

1.3 Permeability

1.3.1 Absolute Permeability

When studying the flow of a fluid in a porous medium, either it is a reservoir or a core sample, it is important to look at a parameter called permeability. Permeability of a porous medium is the medium's capability to transmit fluids through its network of interconnected pores (Zolotukhin, 2000). *Absolute permeability*, which is the rock permeability, is empirical expressed by Darcy's Law:

$$q = -K\frac{A}{\mu}\frac{\Delta P}{L} \tag{6}$$

Where q is the fluid flow rate [cm^3/s], A is the cross-sectional area in the flow-transverse direction [cm^2], μ is the viscosity [cP], L is the length of the porous medium [cm], ΔP is the pressure drop across the length L [bar] and K is the permeability. The minus sign is to denote that the pressure decreases with the direction of flow. Permeability is measured in Darcy [D], which is $0.98692 \cdot 10^{-8}$ cm^2.

The rock permeability is dependent on the effective porosity, the correlation between pore throats and pore volume, pore size distribution and tortuosity of the medium(Lien, 2011). It will also vary in different directions since permeability is regarded as a directional tensor, like parallel to the bedding or perpendicular of the bedding. Absolute permeability is not dependent on fluid type.

1.3.2 Effective and Relative permeability

In a petroleum reservoir the pore space is filled with more than one fluid, for instance oil, water and gas. And if these fluids are immiscible, the ability for each fluid to flow will decrease because of the others presence. Darcy's law can be altered to determine each of the fluid permeabilities with a given saturation:

$$q_i = -K_{e,i}\frac{A}{\mu_i}\frac{\Delta P_i}{L} \tag{7}$$

Where $k_{e,i}$ is the *effective permeability* and *i* denotes each fluid. The sum of the effective permeability is always less than the absolute permeability because of the interference between fluids who shares the same channels (Honarpour, 1988). *Relative permeability* is the ratio between the effective permeability of fluid and the absolute permeability to porous medium.

$$k_{r,i} = \frac{K_{e,i}}{K} \tag{8}$$

Where $k_{r,i}$ is the relative permeability, $K_{e,i}$ is the effective permeability and *K* is the absolute permeability. Relative permeability and effective permeability are both dependent on the fluid saturation, which means it will change as the saturation will change. Figure 1 shows relative permeability curve vs. water saturation

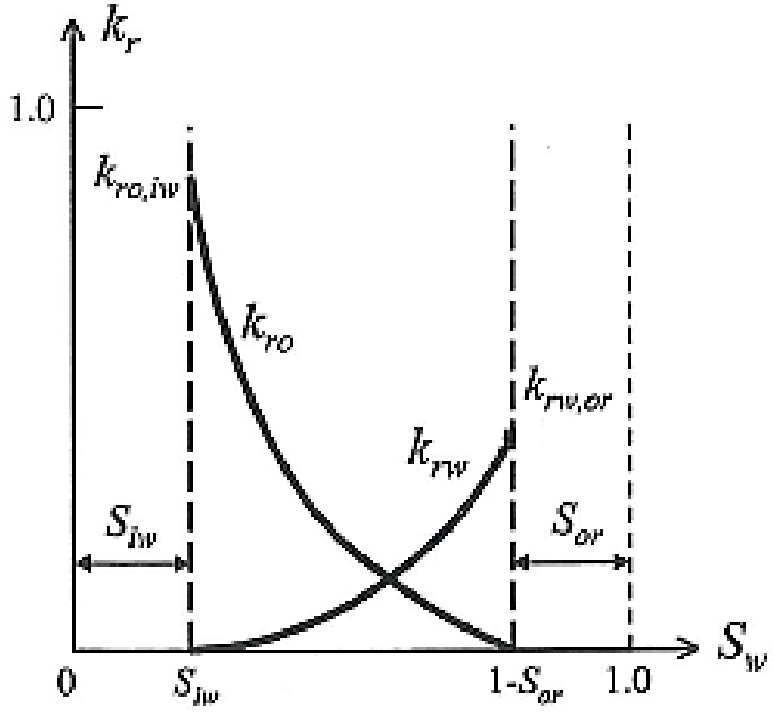

Figure 1: Relative permeability as function of water saturation(Lien, 2011)

1.4 Mobility

Mobility, λ_i, is the ratio between the endpoint effective permeability, $K_{e,i}$, and the viscosity of a fluid, μ_i, and describes how easy the fluid is flowing through a porous medium.

$$\lambda_i = \frac{K_{e,i}}{\mu_i} \tag{9}$$

Mobility ratio, M, is an important parameter when more than one fluid flows in the reservoir. It is defined as the ratio between the mobility of the displacing and the displaced fluid:

$$M = \frac{\lambda_{(displacing)}}{\lambda_{(displaced)}} = \frac{k_{r(displacing)} \cdot \mu_{(displaced)}}{k_{r(displaced)} \cdot \mu_{(displacing)}} \tag{10}$$

1.5 Capillary Pressure

Capillary pressure can be defined as the molecular pressure difference across the interface of two immiscible fluids (Zolotukhin, 2000). It can also be defined as the pressure difference between the non-wetting and the wetting fluid:

$$P_c = p_{nw} - p_w \tag{11}$$

where P_c is the capillary pressure and p_{nw} and p_w are the pressure of the non-wetting and wetting fluids, respectively.

The interface of the two immiscible fluids in a cylindrical tube is curved like in form of a spherical meniscus, Figure 2.

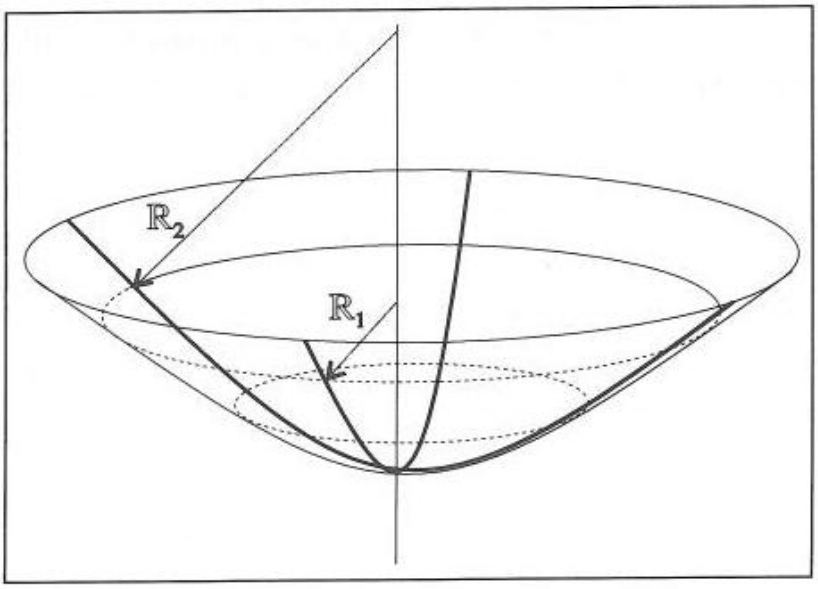

Figure 2: A meniscal surface and the main radii of its curvature, R_1 and R_2(Zolotukhin, 2000)

The capillary pressure for a cylindrical tube is also applicable in pores, and is given by the Laplace equation:

$$P_c = \sigma_{nww}\left(\frac{1}{R_1}+\frac{1}{R_2}\right) \tag{12}$$

Where R1 and R2 are radii of the interface curvature, and σ_{nww} is the interfacial tension between the non-wetting and the wetting fluid. For a hemispherical meniscus, the definition can be expressed as:

$$P_c = \frac{2\sigma_{nww}cos(\theta_c)}{r_c} \tag{13}$$

where θ_c is the contact angle and r_c is the radius to the meniscus.

1.6 Capillary Number

The capillary number N_c is a dimensionless ratio of the viscous forces (VF) to local capillary forces (CF) (Zolotukhin, 2000). Capillary number can be defined different ways, one of them are:

$$N_c = \frac{k\,|\nabla\vec{\phi}|}{\sigma_{nww}\cdot\cos\theta_c} = \frac{VF}{CF} \tag{14}$$

where ϕ is the potential of flow.

According to experimental observations, there is a relation between capillary number and residual wetting or wetting saturations. This relation can be plotted as a curve called capillary desaturation curve (CDC), Figure 3.

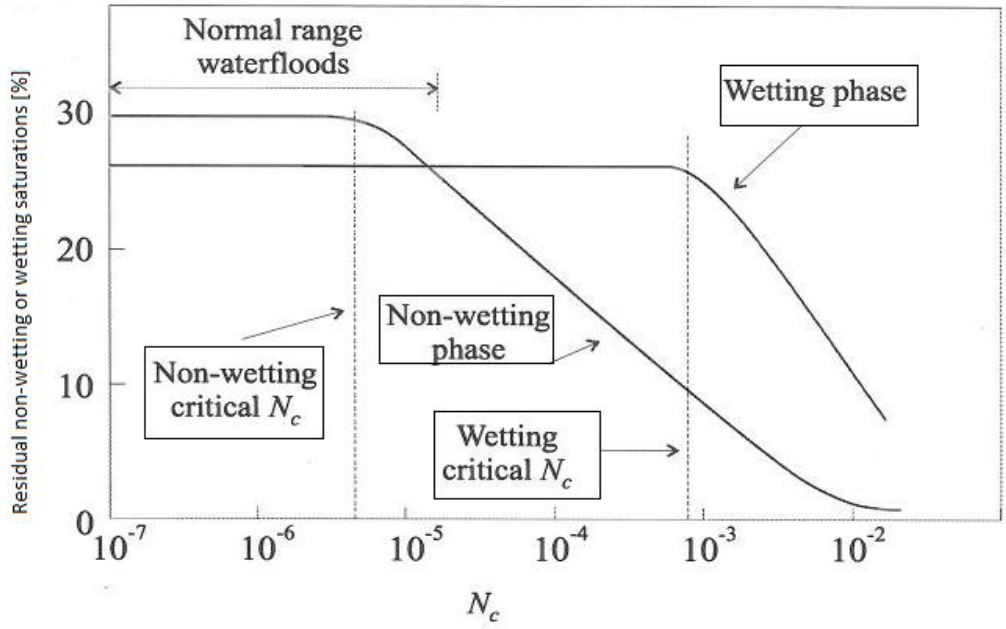

Figure 3: Capillary desaturation curve. Residual saturation as function of capillary number N_c. Modified from (Lake, 1989).

The residual saturation remained unchanged until reaching the critical capillary number. When reaching critical N_c, the residual saturation will decrease as the capillary number increase. There is a big difference between the non-wetting phase and the wetting phase, since the wetting phase need to increase capillary number by hundreds to reach the critical capillary number.

To increase N_c, the viscos force has to increase or/and the capillary force decrease. This can be done by decreasing the interfacial tension between the fluids, which will make more of the trapped oil to be mobile, hence improve the oil recovery.

1.7 Wettability

When two or more immiscible fluids are near a solid surface, the molecules to the fluids will have an adhesive force that attracts them to the molecules of the surface. The fluid with the strongest adhesion, will stick preferentially to the surface and define the wettability of the solid medium. Hence the wettability is defined as “the tendency of one fluid to spread on or adhere to a solid surface in the presence of other immiscible fluids.”(Craig, 1971)

Wettability is crucial parameter when studying reservoir flow, since wettability has been shown to affect the waterflood behavior, relative permeability, capillary pressure, irreducible water saturation, residual oil saturation, dispersion, simulated tertiary recovery, and electrical properties (Anderson, 1987).

In a rock/oil/brine system, wettability is a measure of the preference that the rock has for either the oil or water(Anderson, 1986b). If the rock is water-wet, the water has a tendency contact the majority of the rock surface, especially the small pores. Similarly, oil will have a tendency to contact majority of the rock and the small pores in an oil-wet rock. If the rock does not have any wetting preference, it will be considered as a neutral-wet.

Wettability can also be heterogeneous distributed, which means that some of the rock surface is water-wet and some are oil-wet, like *mixed-wettability*(Salathiel, 1973), which is determined by the pore size, Figure 4. Mixed-wet small pores (MWS) are oil-wet in the small pores and mixed-wet large pores (MWL) are oil-wet in the largest pores. Fractional-wettability(Brown and Fatt, 1956) is uncorrelated to pore-size.

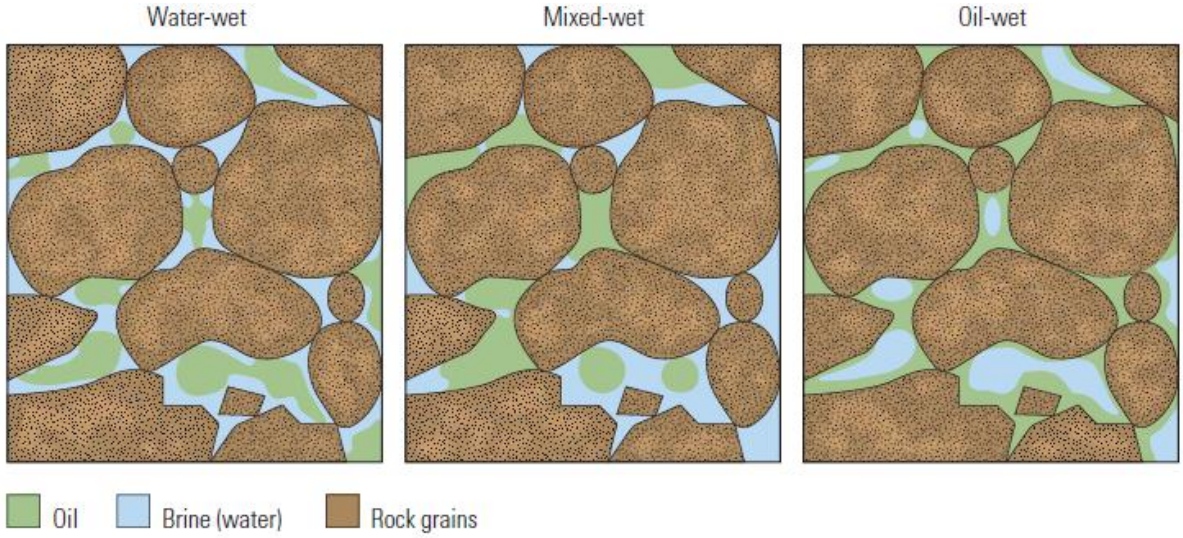

Figure 4: Wetting in water-wet, mixed-wet and oil-wet pores(Abdallah et al., 2007)

The term wettability is used for the wetting preference of the rock and does not necessarily refer to the fluid that is in contact with the rock at any given time(Anderson, 1986b).

Almost all clean sedimentary rocks are water-wet, which means prior to oil-immigration. But the wettability can change by adsorption of polar compounds and/or the deposition of organic matter originally in the crude oil(Anderson, 1986b). The polar compounds contain both a polar end and a hydrocarbon end, which makes the polar end adsorb the rock and the hydrocarbon end to contact the fluids. Some natural surfactants in crude oil are sufficiently soluble in water, and have the ability to adsorb onto the rock.

Wettability Measurement

There are different ways to measure wettability, although none of them are fully accepted, three quantitative measurements are generally used(Anderson, 1986a). *Contact angle method* measure the contact angle on a specific surface, hence not usable for core sample. *Amott-Harvey-method* and *USBM-method (U.S. Bureaus of Mines)* measure the average wettability of a core sample. Only Amott-Harvey method has been used in this thesis.

Amott-Harvey method combines imbibition and forced displacement to measure the average wettability of a core (Amott, 1959). This method is based on that the wetting fluid will generally imbibe spontaneously into the core, displacing the non-wetting one. The Amott-Harvey index is defined as:

$$I_{A-H} = \delta_W - \delta_O = \frac{V_{o,sp}}{V_{o,t}} - \frac{V_{w,sp}}{V_{w,t}} = \frac{S_{w,sp} - S_{iw}}{1 - S_{or} - S_{iw}} - \frac{S_{o,sp} - S_{or}}{1 - S_{or} - S_{iw}} \quad (15)$$

Where δ_W and δ_O is the "displacement by water"-ratio and "displacement by oil"-ratio, respectively. $V_{o,sp}$ and $V_{w,sp}$ is the spontaneous displaced volumes and $V_{o,t}$ and $V_{w,t}$ is the total displaced volumes(Anderson, 1986a).

The Amott-Harvey index varies from +1 to -1, and the wettability is:

- Water-wet: $0.3 < I_{A-H} < 1$
- Neutral-wet:$-0.3 < I_{A-H} < 0.3$
- Oil-wet: $-1 < I_{A-H} < -0.3$

1.8 Imbibition and Drainage

Imbibition is the process where the wetting phase is displacing the non-wetting phase in a porous medium. Conversely, drainage is the process where the non-wetting phase is displacing the wetting phase.

During a waterflood in a water-wet rock, the water will imbibe into the smallest pores, making the oil move to the largest pores. It will also displace the connate water, which is in contact with pore walls, and thereby surround the oil-droplets and make it immobile, see Figure 5a. This is called snap-off and the oil production will almost stop after breakthrough.

During a waterflood in an oil-wet rock, the water will pass through and make it look like fingers, see Figure 5b. The oil will be trapped in the smallest pores and as a continuous film on the rock surface(Donaldson and Thomas, 1971). The oil can be produced after breakthrough with a high water cut and a long production tail.

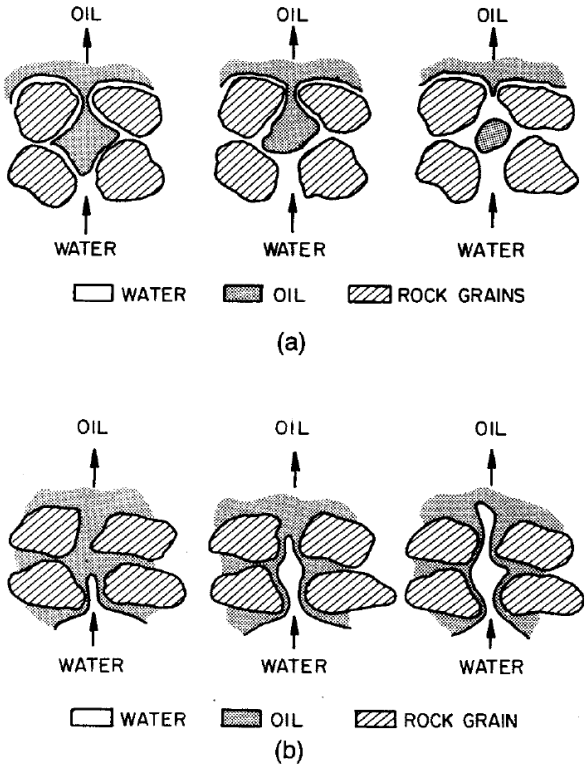

Figure 5: Water flood in a a) strongly water-wet rock and a b) strongly oil-wet rock(Raza, 1968)

1.9 Miscibility

Miscibility between fluids is determined by the electrostatic forces between the molecules within each fluid. If the attraction between the molecules of the same fluid is stronger than with the adjoining fluid, the two fluids are immiscible. Hence, if the attraction between different molecules is the strongest, the two fluids are miscible.

Gas injection into petroleum reservoirs may be miscible, dependent on the gas and reservoir conditions. Injecting miscible gas as an EOR-method has received big attention in the oil industry because the oil is displaced with maximum efficiency and the result is high recoveries. Examples of gases that can be used as a miscible displacement process are enriched hydrocarbon gases, flue gas, nitrogen and CO_2.

Miscible gas displacement can be divided into first-contact miscible process and multi-contact process, and can be explained by the use of a ternary phase diagrams. The corners of the diagrams represent the different fluid-components. Light hydrocarbons (methane) is in

the top corner, intermediate HC in the bottom right corner and heavy oils in the bottom left corner. Each point inside the diagram is a composition of those three and is dependent on the relative distance between the corners and the point. Between the light HC and the heavy HC there is a two-phase region. At the tip of the two-phase region there is a critical line, which decides what kind of miscible process we have.

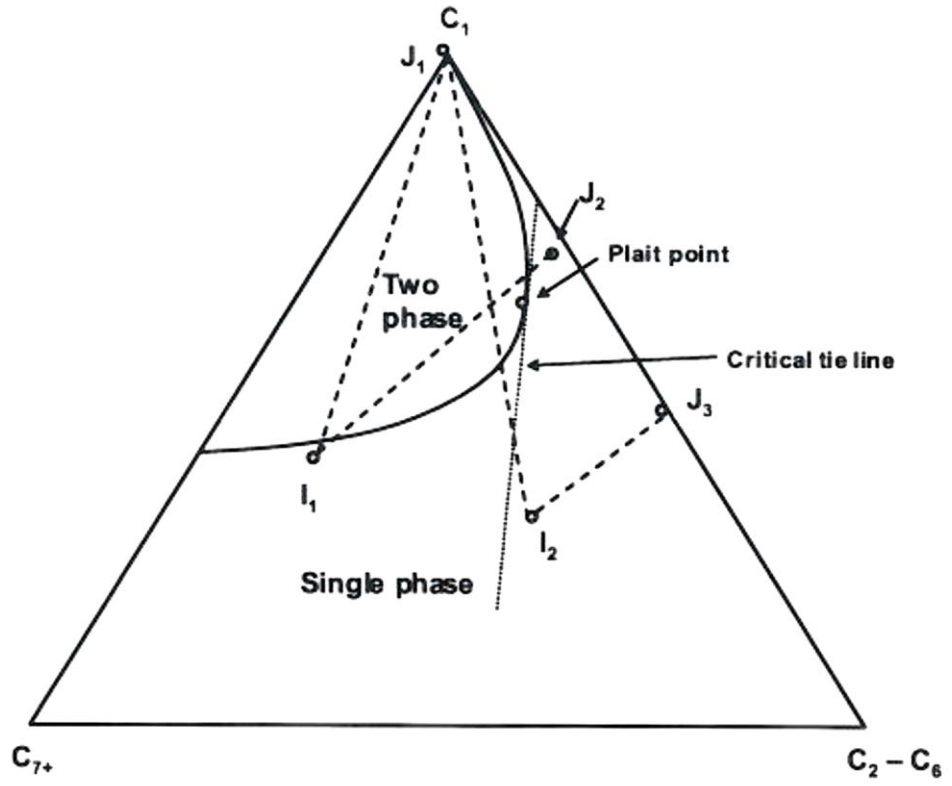

Figure 6: Ternary phase diagram of a C_1, C_2-C_6 and C_{7+} composition. J_1, J_2 and J_3 is the injected gas and I_1, I_2 and I_3 is the reservoir oil composition. Modified from (Skarstad, 2011)

A displacement that occurs entirely within the one phase region is *first-contact miscible*(Skarstad, 2011), and can show by the J3-I2 line. J1-I2 is an example of *a vaporizing gas drive*, which is a multi-contact process. There will be a miscible front between the injected gas and the oil, which is made by the oil vaporizing intermediate components to the gas phase. Another multi-contact process is J2-I1, which is called *condensing gas drive*, where the intermediate HC from the gas is extracted into the oil and makes it lighter, and thereby miscible with the new injected gas. If the line crosses the two-phase region but not the critical line, it is an immiscible process.

Miscibility is not only dependent on the fluid composition, but also reservoir conditions, like pressure and temperature. The pressure determines the two-phase region in the ternary phase diagram. Higher pressure makes the two-phase region smaller, which means that a displacement process that is immiscible can be miscible with higher pressure. The lowest pressure which makes a miscible displacement is called *minimum miscibility pressure*.

1.10 Dispersion

Dispersion can be defined as the mixing of two miscible fluids, caused by diffusion and convection(Lake, 1989). Molecular diffusion is a process of mass transfer and mixing due to the motion of molecules. The driving force is the concentration gradient and the process leads to equilibrium in the concentration distribution. Fick's second law describes the unsteady state diffusion in one dimension between two miscible fluids.

$$\frac{\partial C}{\partial t} = D_o \frac{\partial^2 C}{\partial x^2} \tag{16}$$

where C is the concentration, t is the time, D_o is the effective diffusion coefficient and x is the travel distance. The diffusion coefficient is given with the absence of a porous media, which will make it larger than in the presence of a porous media. This can be altered with the correlated diffusion coefficient, D.

$$\frac{D}{D_o} = \frac{1}{F\Phi} \tag{17}$$

where F is the formation electrical resistivity and ϕ is the porosity. Convection happens when the fluid is flowing through the same porous media and particles are mixing on a micro scale. The increased mixing depends on the interstitial velocity. Perkins and Johnston have defined three flow regimes and are shown in Figure 7, where the x-axis is the Pèclet number which is the ratio of convection and diffusion. With low Pèclet number the diffusion controls the flow, with high number the convective dispersion controls the flow.

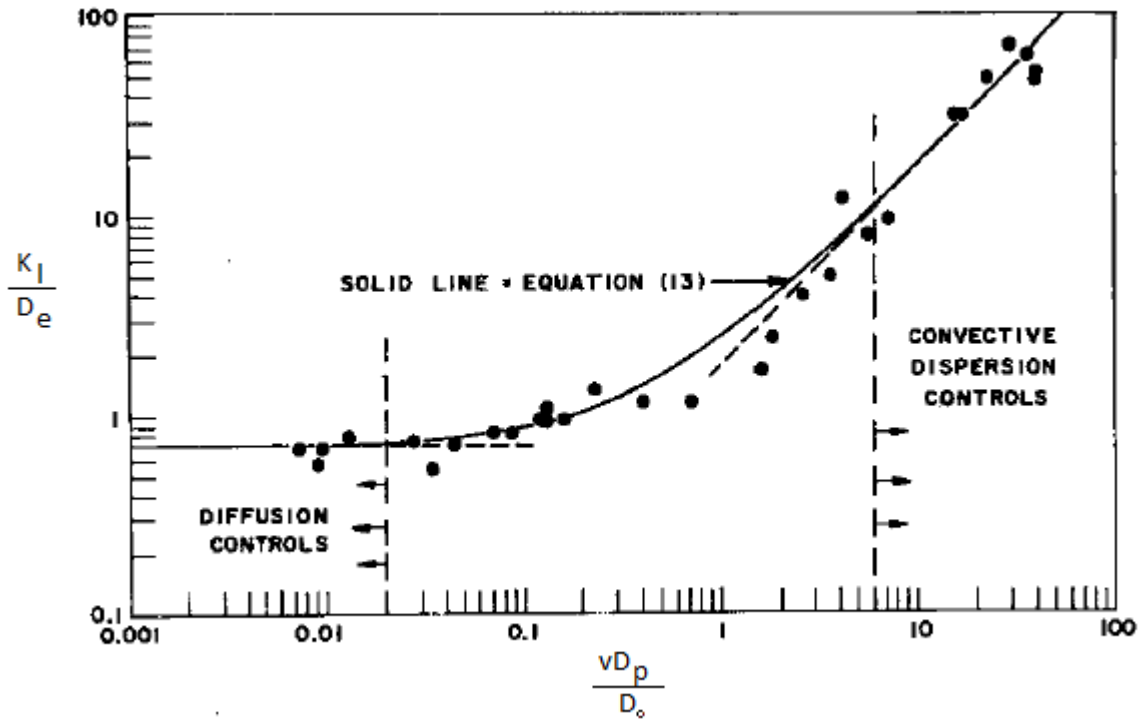

Figure 7: Longitudinal dispersion coefficient in a permeable media flow. K_l is the longitudinal dispersion coefficient [cm^2/sec], D_o is the molecular diffusion coefficient [cm^2/sec], v is the average interstitial velocity [cm/sec] and D_p is the average diameter of the particles.

2 CO_2

CO_2 is the primary greenhouse gas emitted through human activities and accounted for about 84% of all U.S. greenhouse gas emissions from human activities in 2011. CO_2 is naturally present in the atmosphere as part of the Earth's carbon cycle, which is altered by human activities - both by adding more CO_2 to the atmosphere and by influencing the ability of natural sinks, like forests, to remove CO_2 from the atmosphere(EPA, 2012).

While CO_2 emissions come from a variety of natural sources, human-related emissions are responsible for the increase that has occurred in the atmosphere since the industrial revolution. CO_2 concentration has increased from 320 ppm to 400ppm the last 65 years according to the Keeling curve(Scripps Institution of Oceanography, 2013).

2.1 Physical Properties of CO_2

It is important to know the properties and phase behavior of CO_2 when flooding. Figure 8 shows the phase diagram for CO_2, including sublimation point, triple point and critical point.

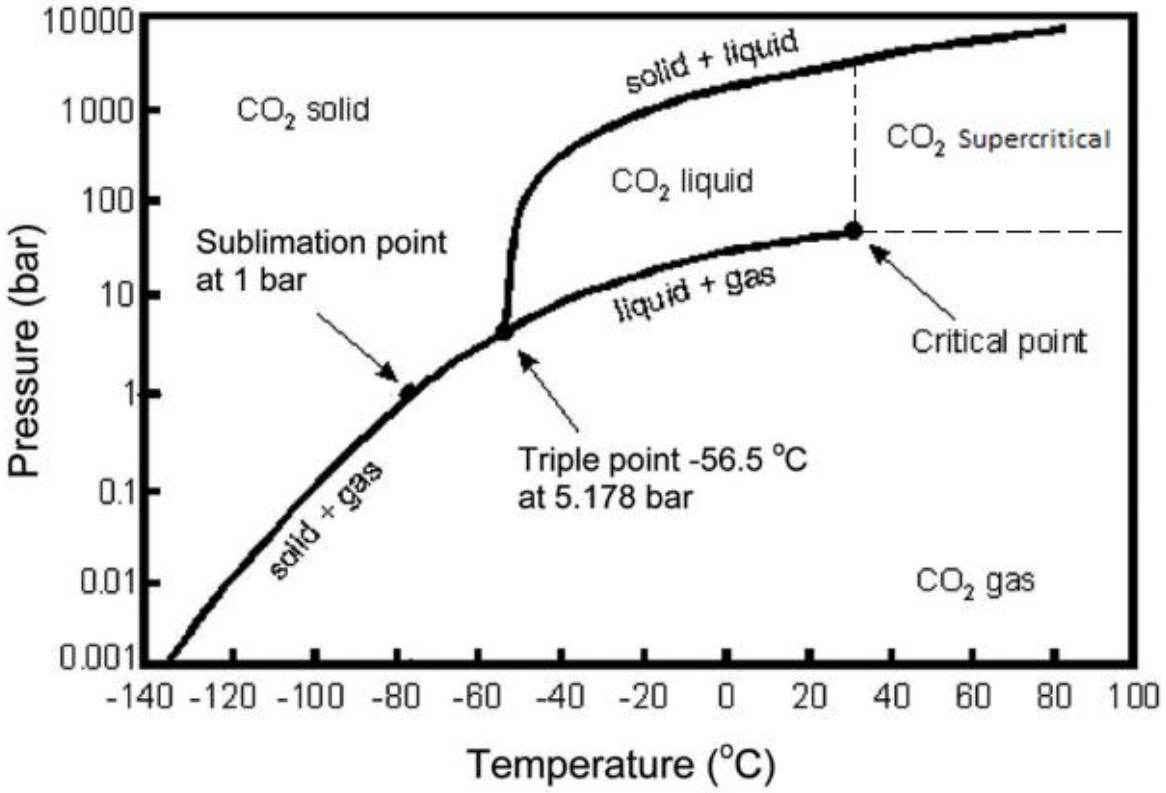

Figure 8: Phase diagram for CO_2, including the sublimation point, triple point and critical point. Modified from (ScienceDirect, 2011)

The critical temperature is 31.08°C, which means that the CO_2 will be in a supercritical state regardless of the pressure above this temperature. The pressure that corresponds to the critical temperature is 73.82bar. Above this critical condition, pure CO_2 cannot be liquefied. For this thesis the CO_2 is in room temperature (20°C) and is pressurized to 85-100bar, which means the CO_2 is always liquefied but close to the supercritical zone.

Figure 9 and Figure 10 shows the CO_2 density and viscosity for different pressure and temperature. Under the critical temperature, the increase in density and viscosity change slowly until reaching the liquid-gas line where it makes a big jump before flattening out. Above the critical temperature, density and viscosity does not get at rapidly transition when reaching the same pressure.

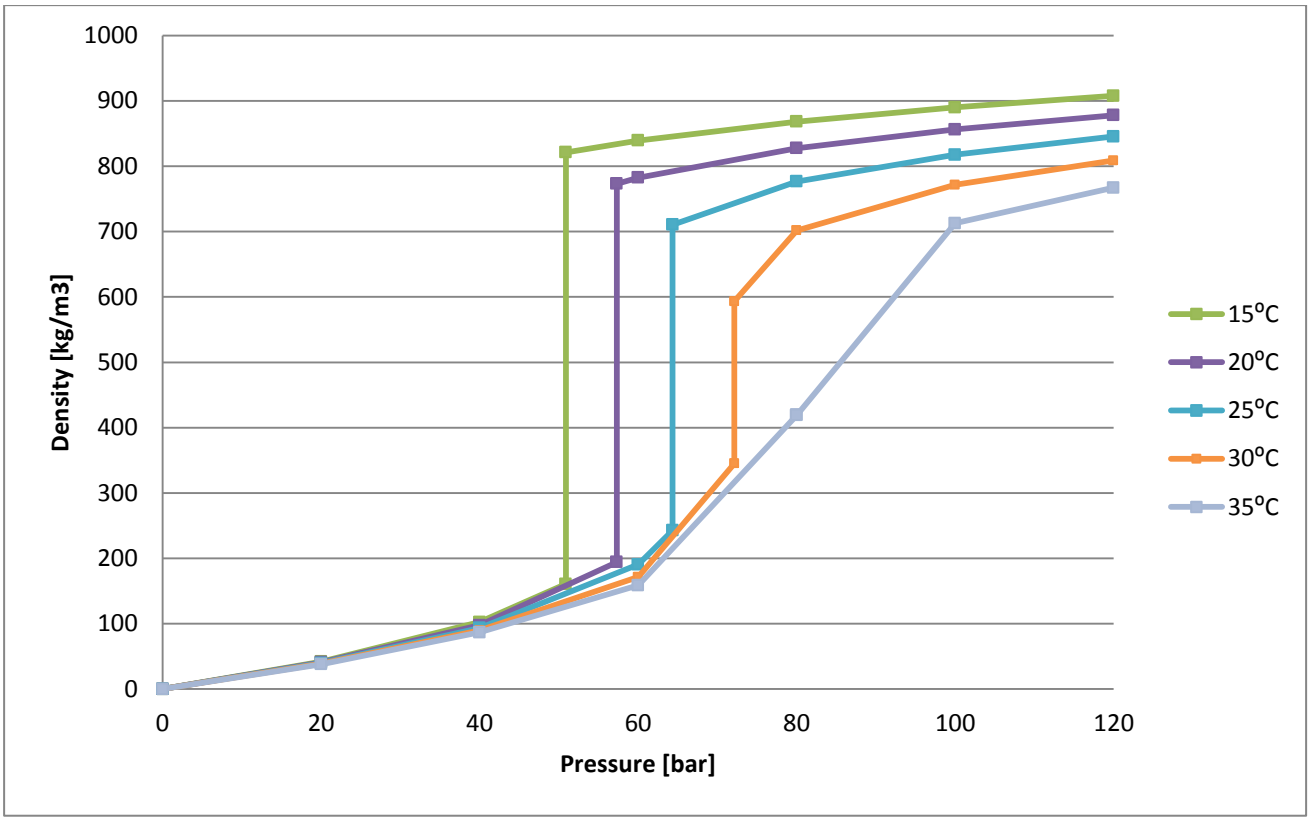

Figure 9: CO_2 density as function of pressure at various temperatures. Modified from (NIST, 2012)

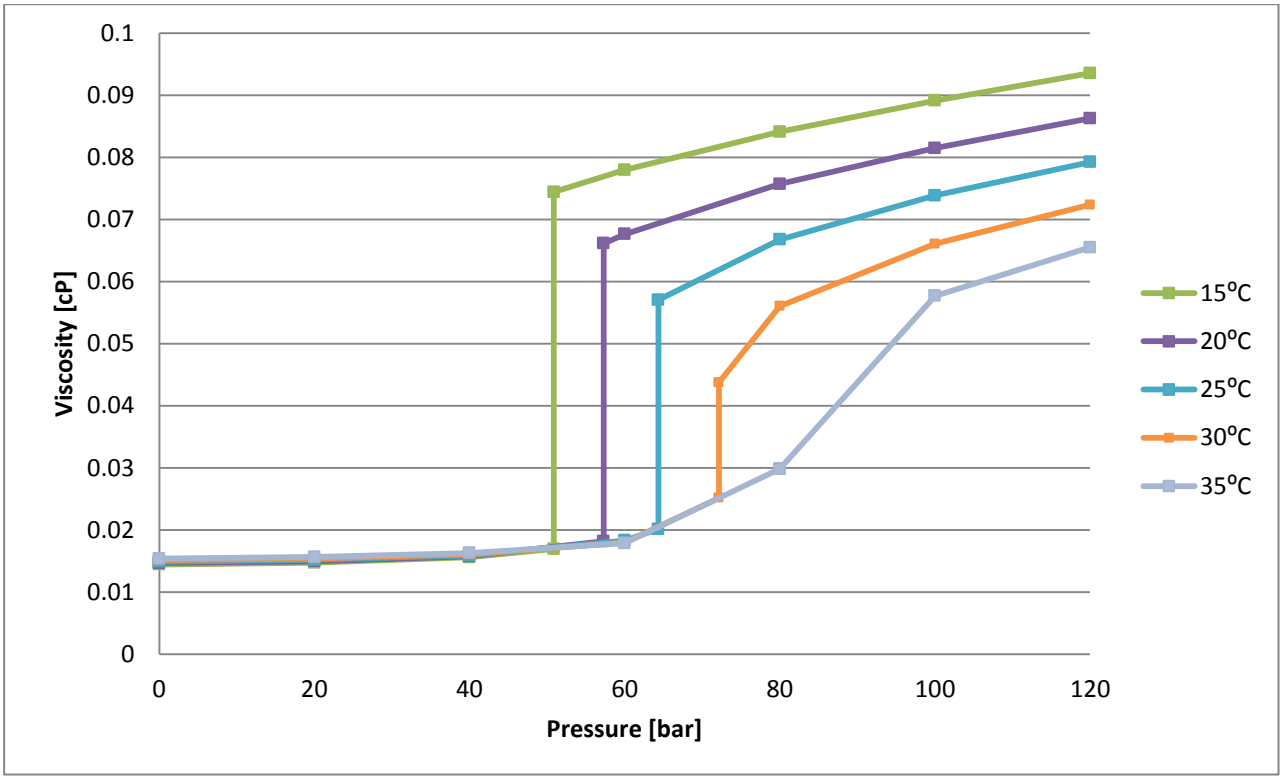

Figure 10: CO_2 viscosity as function of pressure at various temperatures. Modified from (NIST, 2012)

2.2 EOR from CO_2 injection

Injection of CO_2 into oil fields has many beneficial purposes, including production of methane from natural gas hydrates (Thomas, 2001), for carbon sequestration (Oldenburg, 2000) and enhanced oil recovery. The primary purpose of miscible CO_2 flooding for EOR is to mobilize the oil and to reduce the residual oil saturation.

The advantages of CO_2 as miscible flooding is that it promotes oil swelling, reduces oil viscosity, increases oil density, it is soluble in water and can extract and vaporize portions of the oil. Compared to other miscible gases, CO_2 can extract heavier components (up to C_{30}) and achieve miscibility at lower pressures (100 to 300bar)(Schechter et al., 1998).

Some of the disadvantages of CO_2 are the macroscopic displacement due to the mobility ratio of the CO_2, crude oil and brine, which makes the displacement front unstable causing viscous fingering of CO_2. Vertical displacement efficiency may also be low due to gravity segregation. CO_2 can also dissolve into brine and make carbonic acid, which may weaken the reservoir rock and corrode well and production plant (Saadawi et al., 2011).

Even though the reservoir has favorable criteria for CO_2 flooding, the economics may not be. Total CO_2 costs (both purchase price and recycle costs) can amount to 25 to 50 percent of the cost per barrel of oil produced. This is due to the lack of availability of carbon dioxide and the high amounts needed. Installations of CO_2 recycle plant and corrosion resistant field production infrastructure, and laying CO_2 gathering and transportation pipelines will also increase the cost(NETL, 2010).

3 Foam

Even though gas injection has a high microscopic sweep and can mobilize almost all of the trapped oil it contacts, the volumetric sweep and gas utilization is poor. This is due to viscous fingering and gravity segregation which is due to rock heterogeneity and the gas density and viscosity (Lake, 1989). This can be resolved by injecting surfactants and make with gas, or alternating with gas (SAG), and thereby create foam (Kovscek et al., 1993, Rossen, 1996, Farajzadeh et al., 2009).

Foam can affect the oil recovery in three ways, compared to gas or WAG (water alternating gas) flooding (Farajzadeh et al., 2010, Andrianov et al., 2011)

(1) by stabilizing the displacement process as the displacing fluid (gas or foam) viscosity increase;
(2) by blocking the high-permeable swept zones and diverting the fluid into the unswept zones; and
(3) by reducing the capillary forces via reducing the interfacial tension due to the presence of surfactant

Interfacial mass transfer between gas and oil will mobilize the oil-in-place by dissolution, viscosity reduction and swelling (Nobakht et al., 2008). Foam also has a selective mobility, which means it has lower mobility in a high-permeable layer and, consequently, will be effectively blocking /hindering the flow in these layers in favor of low-permeability (Farajzadeh et al., 2012).

3.1 Definition

Foam has been described as an “agglomeration of gas bubbles separated from each other by thin liquid films.”(Bikerman, 1973). The surfactant-stabilized films, or lamellae, are in the order of 10-100nm and can be treated as mathematical surfaces. The surface area of foam is proportional to the energy of the system, where the surface tension is the constant of proportionality. Where lamellae touch a solid or each other, a liquid-filled, prismatic region called the plateau border forms. The width of this region is dependent on the capillary pressure. If the capillary pressure increases the lamellae thickness decreases until it reach the critical thickness h^{cr}, which will make the lamellae collapse (Figure 11). (Rossen, 1996). Disjoining pressure is the difference between the pressure in a region of a phase adjacent to a surface confining it, and the pressure in the bulk of this phase(Aronson et al., 1994).

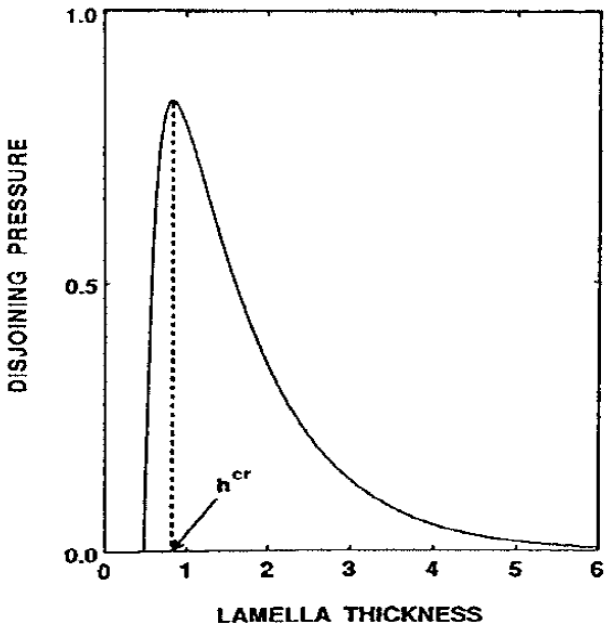

Figure 11 Disjoining pressure as a function of lamella thickness.(Jimenez, 1989)

such that the liquid phase is continuous (i.e., connected) and at least some part of the gas is made discontinuous by thin liquid films called lamellae (Falls et al., 1988). This definition works for both bulk-foam, which are foam with bubble-sizes that are much smaller than the dimension or pores, and individual-lamellae foams. Individual-lamellae exist when the bubble radius is much bigger than the pores, and each lamellae separate two bubbles (Hirasaki and Lawson, 1985).

Foam can also be classified as a continuous-gas foam and a discontinuous-gas foam. A continuous-gas foam is one which there exist at least one pathway for gas flow in pore network that is unblocked by lamellae. A discontinuous-gas foam is one in which all pathway for gas flow are blocked by lamellae (Figure 12).(Rossen, 1996)

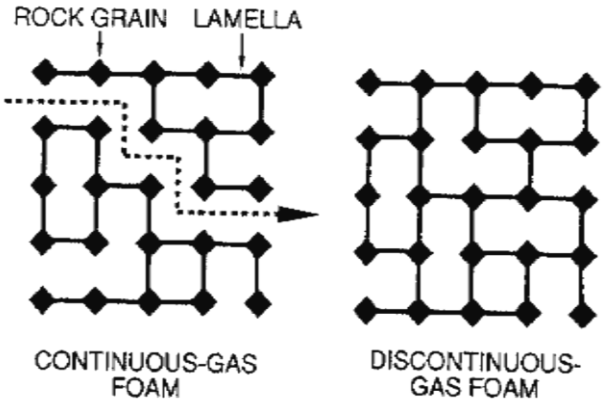

Figure 12 Schematics of continuous-gas and discontinuous-gas foams. (Rossen, 1996)

It is practically impossible to differentiate continuous-gas and discontinuous-gas foam in a porous media, since one cannot verify the position, movements or even the existents of lamellae inside the rock. Rossen has thereby defined foam in porous media "that which reduces gas mobility in the presence of an aqueous solution of surfactant below that observed at the same saturation of water". He also conclude with that "foams in porous media are composed of individual liquid lamellae each straddling a pore body or throat and separated from each other by at least a pore length".

When gas and surfactant are injected at the same time it creates foam. The ratio between the gas-rate, u_g, and the total flow-rate for surfactant, u_s, and gas is defined as the foam quality, f_g.

$$f_g = \frac{u_g}{u_g + u_s} \tag{18}$$

If the foam quality is higher than 90%, the foam is considered as dry foam.

3.2 Foam Generating

When foam flows, individual lamellae are destroyed, and others created, continually. The process where lamellae creation proceeds continually is distinct from foam generation, which is the initial creation of foam from gas and surfactant solution. In experiments, foam generation is inferred from a drop in gas mobility during gas flow through a porous medium. The process of foam generation is dependent of the injection method, but also by the injection rate and foam quality (Figure 13). The gas velocity has to be higher with drier foam. In steady liquid/gas injection, there is a minimum ∇p for foam generation, which increases with increasing foam quality.

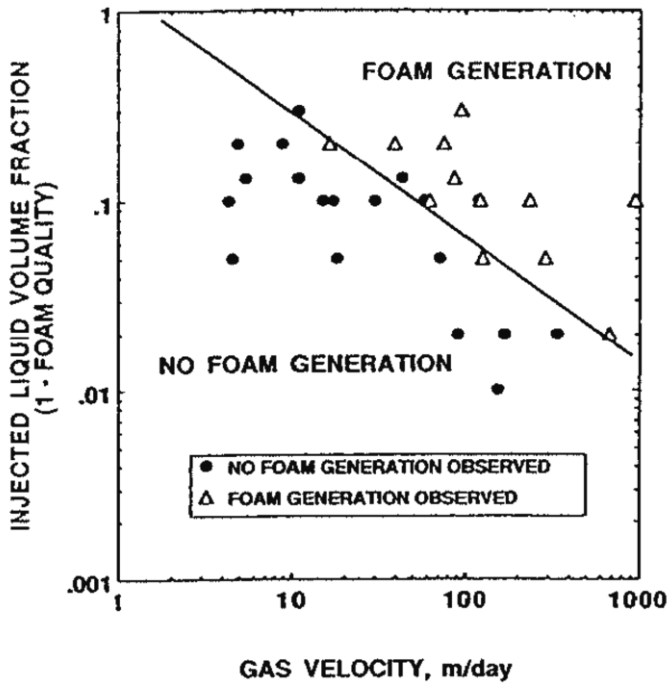

Figure 13: Condition of foam generation in steady gas/liquid flow. (Friedmann et al., 1991)

3.3 Mechanisms of Lamella creation

There are four ways to create lamellae in porous media:

(1) Leave Behind

As gas invades a previously liquid-saturated region, it goes through the many interconnected flow channels. Often, two gas fronts approach the same liquid-filled pore space from different directions and the liquid in the pore space is squeezed into a lamella by the two fronts (Ransohoff and Radke, 1988). This is illustrated in Figure 14.

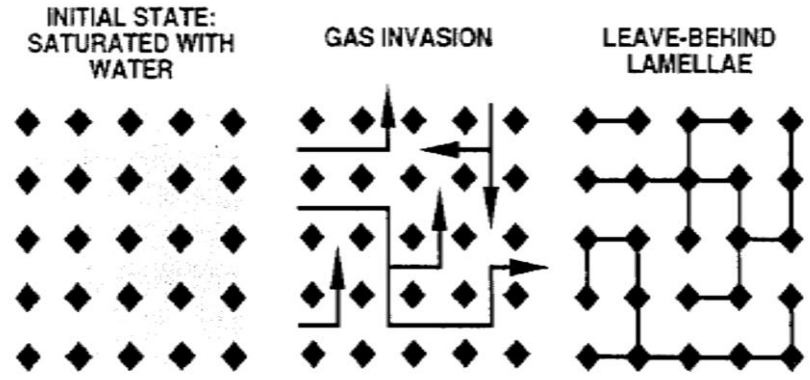

Figure 14 Schematics of leave-behind. (Rossen, 1996)

(2) Snap-off

As a gas bubble expand in a porous media, the capillary pressure decreases and causing a pressure gradient. At sufficiently low Pc, the collar will swell and bridges the throat, thereby blocking the gas flow and leading to the creation of a lamella. (Figure 15)

Figure 15: Schematics of snap-off in a pore-throat. (Rossen, 1996)

(3) Lamellae Division

Lamellae division is different from the others since it already needs lamellae to create more. When a moving lamella enters a pore body with several pore throats, the lamella must stretch across the pore body and either break or deposit a new lamella in each unblocked pore throat (Figure 16).(Ransohoff and Radke, 1988)

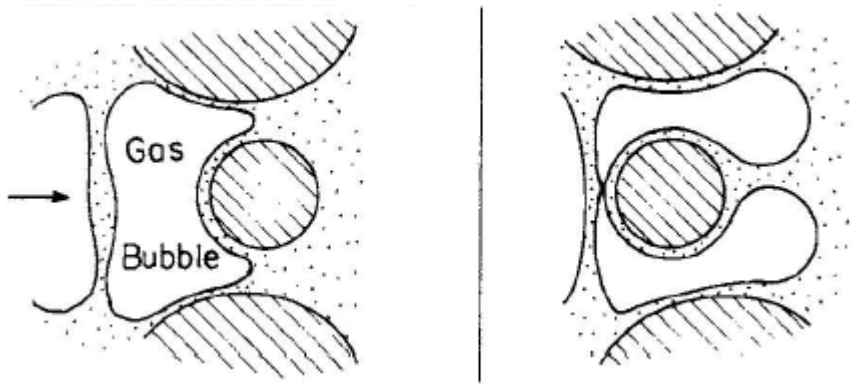

Figure 16: Schematics of the lamella division mechanism.(Ransohoff and Radke, 1988)

(4) Gas Evolution Within Liquid

If a gas is generated by a surfactant within a porous medium chemically or physically, foam is created. Since it needs a high foam-quality to be effective at reservoir conditions, a lot of gas has to be produced from the surfactant.

3.4 Foam Stability and Propagation

When foam is used a reservoir to modify the gas mobility or plug some area, it needs to be stable long enough to result in a better recovery efficiency. The lifetime of foam is dependent on the stability of each lamella, which is dependent of the surfactant concentration, salt concentration, adsorption kinetics, gravitational drainage, gas diffusion through foam films, surface forces, capillary pressure and mechanical fluctuations (Aronson et al., 1994).

Foam propagation is mainly dependent on the surfactant propagation, since the surfactant has to fill the liquid-saturated pore space and also satisfy loss mechanisms to the reservoir rock and residual oil by adsorption. From field experiments the foam propagation is much less than surfactant propagation further away from the well-region, which is where foam generation does not happen because of the rate of the fluids (Rossen, 1996).

3.5 Foam Regimes

In a porous media foams exist in three regimes, dependent on the applied pressure gradient. The regimes are (Gauglitz et al., 2002, Kam and Rossen, 2002):

- Coarse-foam regime: at low pressure gradient
- Transient-foam regime: intermediate pressure gradient
- Strong-foam regime: at high pressure gradient

Coarse-foam regime has low pressure gradient and relatively high gas mobility. The transient-foam regime appears to be unstable with intermediate pressure gradient. Strong-foam regimes, with low gas mobility, can be divided into two flow-regimes depending on foam quality and other factors (Alvarez et al., 2001).

With *high-quality foam*, the pressure gradient depends only upon liquid flow rate and is independent of gas flow rate. There is a limiting capillary pressure where foam will collapse, P_c^*. Low-quality foam is foam with low gas volume fraction. The pressure gradient depends only upon gas flow rate and is independent of liquid flow rate.

3.6 Foam as EOR

Foam as an EOR method has in general two main purposes, plugging and mobility control. Plugging is performed close to the injection and production wells and has a purpose to block the unproductive and high permeable layers to increase the sweep efficiency. It is considered to be the cheapest and easiest method, since it demands less foam. The purpose of using foam as a mobility control is to reduce the high mobility effect of gas by increase the gas viscosity and relative permeability. This will minimize viscous fingering, gravity override and also gas channeling through the thief-zones(Falls et al., 1988, Rossen, 1996). Figure 17 shows the difference between a free gas flood and a foamed gas flood.

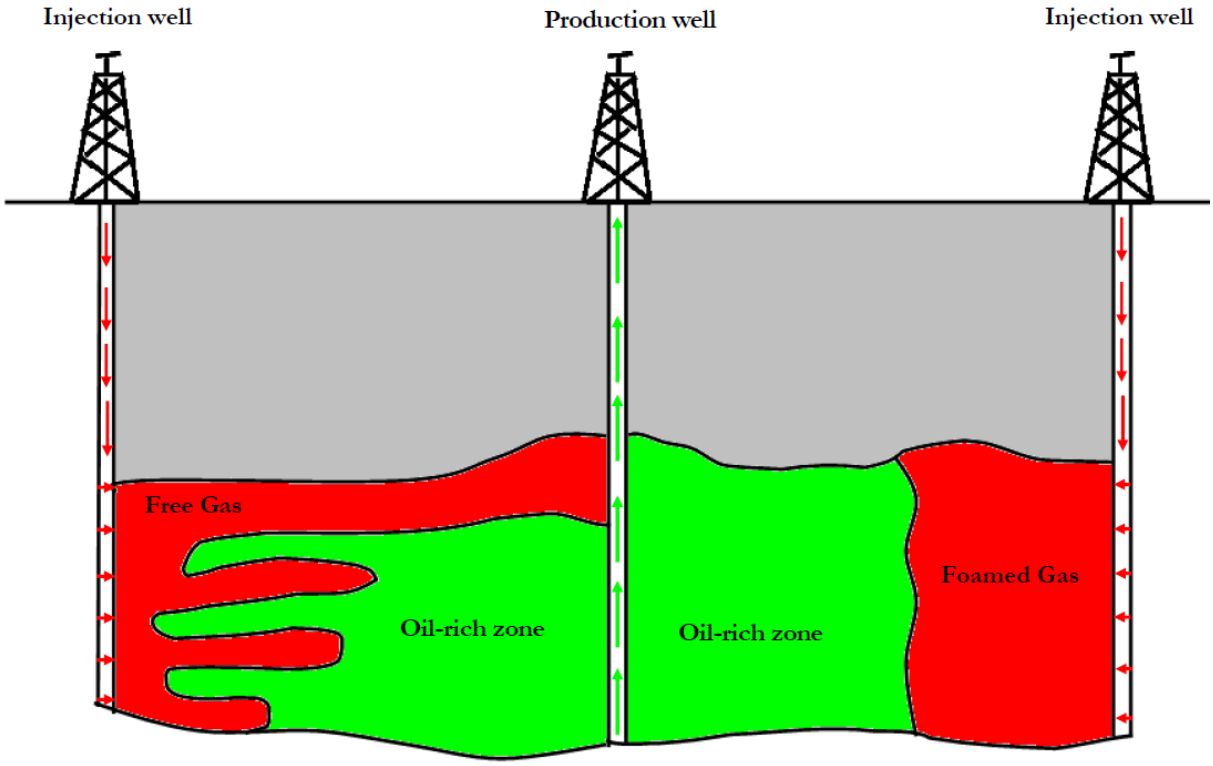

Figure 17: Schematics of foam injection compared to gas injection(Farajzadeh et al., 2009)

Foam as an EOR method has a big potential to give high rewards, especially in carbonate reservoirs where there are a lot of fractures in the low-permeable rock (Srivastava and Nguyen, 2010). Even though there is a big potential and there has been some very positive field-test, the method has not been used very much. There have been used different kinds of gases in the field tests, as steam, N_2, hydrocarbon gas and CO_2 (Turta and Singhal, 2002).

In 1997 there was a pilot-project at the Snorre-field to see if FAWAG (foam assisted WAG) could enhance the oil-production. Until this, WAG had been the main drive mechanism of the field which had led to an early gas breakthrough and high gas-oil ratio (GOR). It was initiated as a gas shut-off production well treatment, thereafter as two large-scale gas

mobility control process. The results showed a significant lower GOR compared to the pre-foam process, and the tracer data indicated a delayed gas breakthrough. 2000 tons of surfactant, AOS $C_{14/16}$, and an investment of 1 million dollars was used in the project. Additional oil recovery value was ~25-40M USD(Skauge et al., 2002).

There have also been done some field tests with CO_2-foam. A field test in New Mexico and 4 tests in San Andres in west Texas, where lower GOR and increased oil recovery has been confirmed(Hoefner et al., 1995, Stevens et al., 1992). None of this field-test has focused on the diffusion-effect of CO2, which could be a factor according to lab-experiments(Nonnekes et al., 2012).

4 Experimental Procedures

4.1 Rock Material

During core analysis it is possible to use either reservoir core or outcrop core. Using reservoir core is expensive and time-consuming because of drilling, and the pressure and temperature conditions are being altered when taken up to the surface.

In this thesis Edwards limestone, which has been collected from Garden City in Texas, has been used. Figure 18 shows a thin section of Edwards limeston. The Edwards is a grainstone that contains wellsorted fossil shells cemented by sparry calcite. The porosity of this rock includes intraparticle, moldic, and a minor amount of intercrystal porosities. The porethroat size is relatively narrow, with a range of 0.1-10µm, compared to the pore bodies which are 50-60 times bigger.(Morrow, 2006)

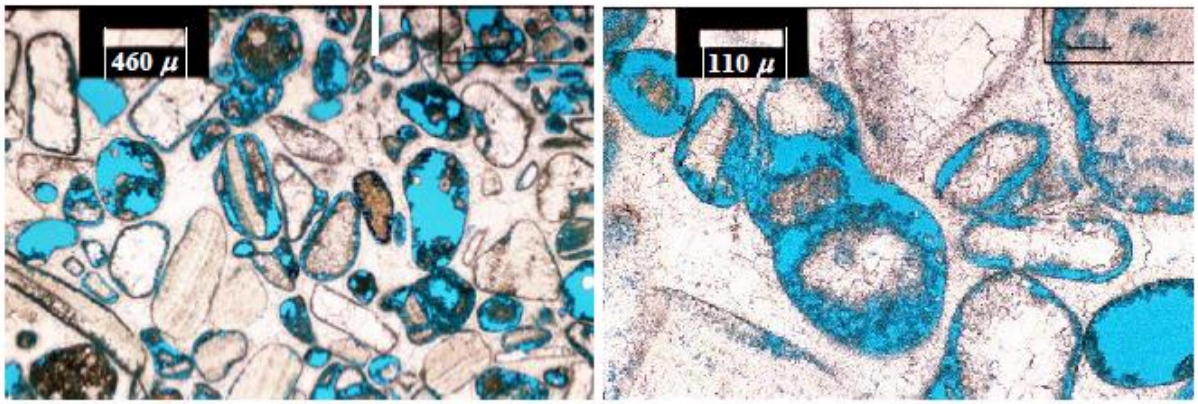

Figure 18: Thin section of Edwards Limestone, from (Morrow, 2006).

The core samples used in this thesis are cylindrical, with a diameter of 2 inches and length of about 7 cm.

4.2 Fluids

A brief summary of all fluids used during this work is presented in Table 1.

Table 1: Fluid properties. (NIST, 2012)

Fluid	Contents	Density 20 °C [g/cm^3]	Viscosity 20°C [cP]	Comments
Synthetic Ekofisk brine	Destilled water	1.05	1.09	Added 0.5 cm^3 NaN_3 to avoid bacterial growth
	4 weight percent NaCl			
	3.4 weight percent $CaCl_2$			
	0.5 weight percent MgCl			
n-Decane	$C_{10}H_{22}$	0.73	0.91	Purity 95%
Decaline	$C_{10}H_{20}$	0.896	0.85	Purity: 95%
Ekofisk Crude	53 weight percent saturated HC	0.85	14.3	Acid number: 0.09
	35 weight percent aromatic HC			Base number: 1.79
	12 weight percent Rasins			
	0.9 weight percent Asphaltenes			
Surfactant: AOS C14/16	Ekofisk brine	N/A	N/A	37% active concentration
	1 weight percent P-C1			
Liquid CO_2	> 99.9999% CO_2	0.8432	0.07877	From NIST database [20°C, 95 bar]

4.3 Core plug preparation

Prior to the experiments, the core plugs were drilled out from a larger slabs of outcrop rock with a hallow cylinder bor. Afterwards they were prepared and general parameters such as, porosity, permeability and wettability were measured. The experimental procedures are described below.

4.3.1 Porosity Measurement

After the core plugs were drilled out they were placed in a heating cabinet, at 80 °C, for at least 24 hours to dry. The core dimensions and dry weight was measured, and the core placed in containers as shown in Figure 19 to be saturated with Ekofisk brine. The core and brine were separated from each other by valves and vacuum evacuated to <600 mTorr. Before the valves between the brine and core were opened and the brine imbibed into the core until equilibrium was reached. The saturated cores were then weighted again.

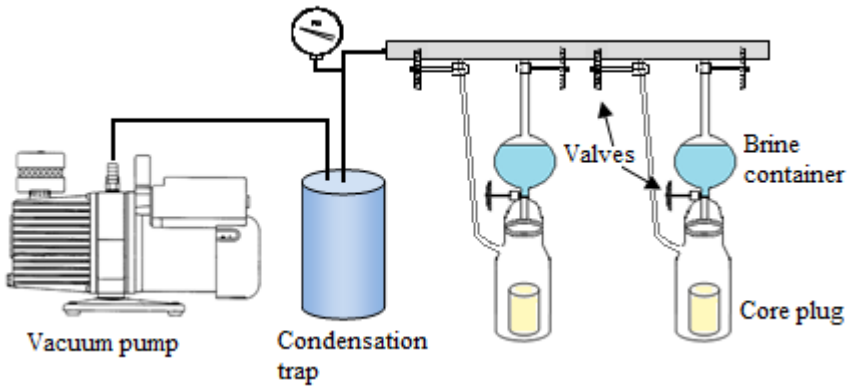

Figure 19: Schematic illustration of the porosity setup.(Haugen, 2012)

The effective porosity was measured by modifying equation (1).

$$\Phi = \frac{V_p}{V_b} = \frac{(m_s - m_d)}{\rho \cdot V_b} \cdot 100 \qquad (19)$$

where m_s and m_d are the weight of the saturated core and the dry core, accordingly, and ρ is the density of the brine.

To measure porosity for core plugs with 100 % saturated oil, n-decane was used instead of Ekofisk brine.

4.3.2 Permeability Measurement

The absolute permeability was measured by flooding the fully brine saturated cores with brine using three constant injection rates, q, ranging from 100 to 1500 cm^3/h for whole cores and 1000-2000 cm^3/h for fractured cores, Figure 20. The pressure drop, Δp, across the core was then recorded and plotted against the injection rate. A regression curve was made, and permeability was calculated using Darcy's law and the line slope curve. The confinement pressure was 10bar above the pressure drop at all times.

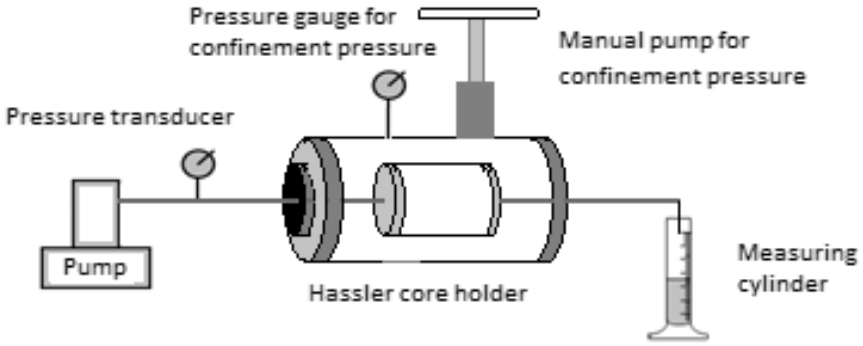

Figure 20: Schematic illustration of the permeability setup.

To measure permeability for core plugs with 100% saturated oil, n-decane was used instead of brine.

4.3.3 Primary drainage

After the permeability measurements, the cores were drained by injecting n-decane with a constant pressure at 1.5bar per cm length of the core until no additional water was produced. This was performed horizontally and at room-temperature. The water saturation (irreducible) and average oil saturation were calculated by material balance.

4.3.4 Wettability Alteration

Outcrop core plugs are generally strongly water-wet, because they never been in contact with crude oil. To study the influence of wettability effects on Edwards' limestone, some of the cores were aged in a North Sea crude oil by the technique used by Graue and Aspenes called dynamic aging method(Graue et al., 1999, Aspenes, 2003). The core plugs were injected with crude oil at a low constant rate and high temperature to allow the polar components in the crude oil, like resin and asphaltene groups, to alter the wettability. A schematic of setup used for aging is presented in Figure 21.

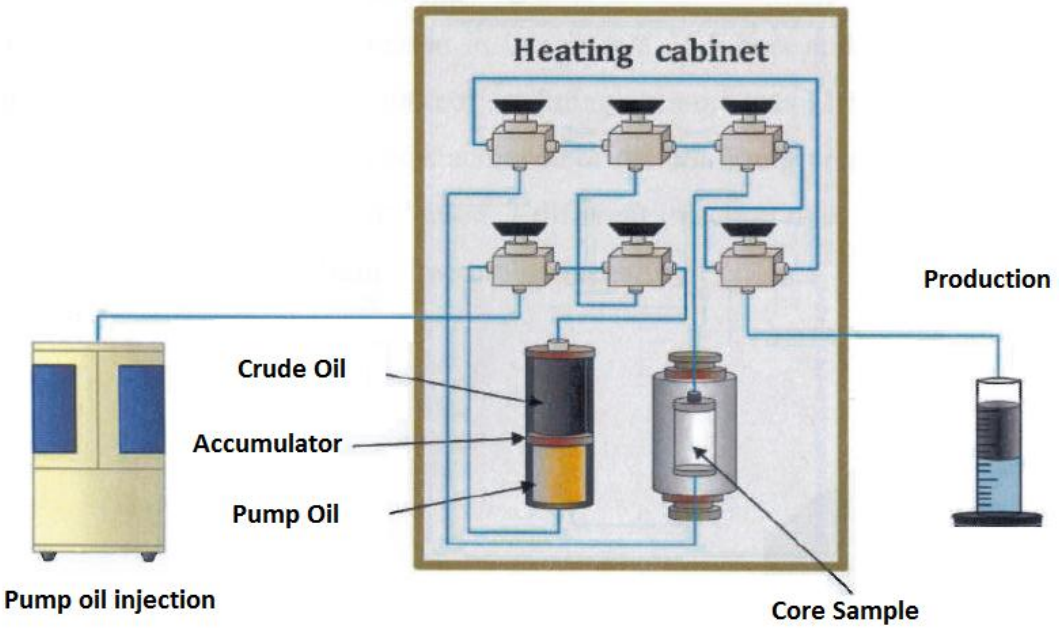

Figure 21: Schematics of the set up used for aging the core(Mani, 2011).

Before the aging process, the crude oil was filtrated through the short chalk filter at a low rate to remove impurities that could block pore throats. The crude oil was filtrated at 80 ^{o}C and the filter was replaced when the differential pressure acceded 20bar due to blockage. The filtrated oil was stored in closed containers in a heating cabinet at the same temperature until used to avoid wax precipitation.

During aging, 100 % water saturated core plugs were installed vertically in a Hassler core holder inside the heating cabinet, which had a temperature of 80 ^{o}C, and filtered crude oil was injecting through the core. The core was drained with 2.5 PV of filtered crude oil in each direction, to eliminate end-effects, and pressure drop was set at 1.5bar/cm. The process was stopped when no additional water was produced. After irreducible water saturation was reached, the injection rate was set at a constant value of 3cm^3/h and maintained for 2 – 4 days in each direction.

After the aging, the crude oil was miscible displaced with 5 PV of decahydronaphtalene (decaline), to prevent the precipitation of asphaltene, and then 5 PV of n-decane. The cores were then cooled to room-temperature.

4.3.5 Wettability Measurement

Wettability was measured by the Amott-Harvey wettability test(Amott, 1959), described in chapter 1.8. The measurement was performed in 4 steps:

1. Spontaneous brine imbibition, where the cores were kept in graduated imbibition cells Figure 22a with brine for 2 weeks. The oil production vs. time was measured.
2. Forced brine imbibition, where brine was injected with 1.5bar/cm, in a Hassler core holder, until oil stopped producing.
3. Spontaneous oil imbibition, where the cores were kept in imbibition cells Figure 22b filled with n-decane for 2 weeks. The water production vs. time was measured.
4. Forced oil imbibition, where oil was injected with 1.5bar/cm, until water stopped producing.

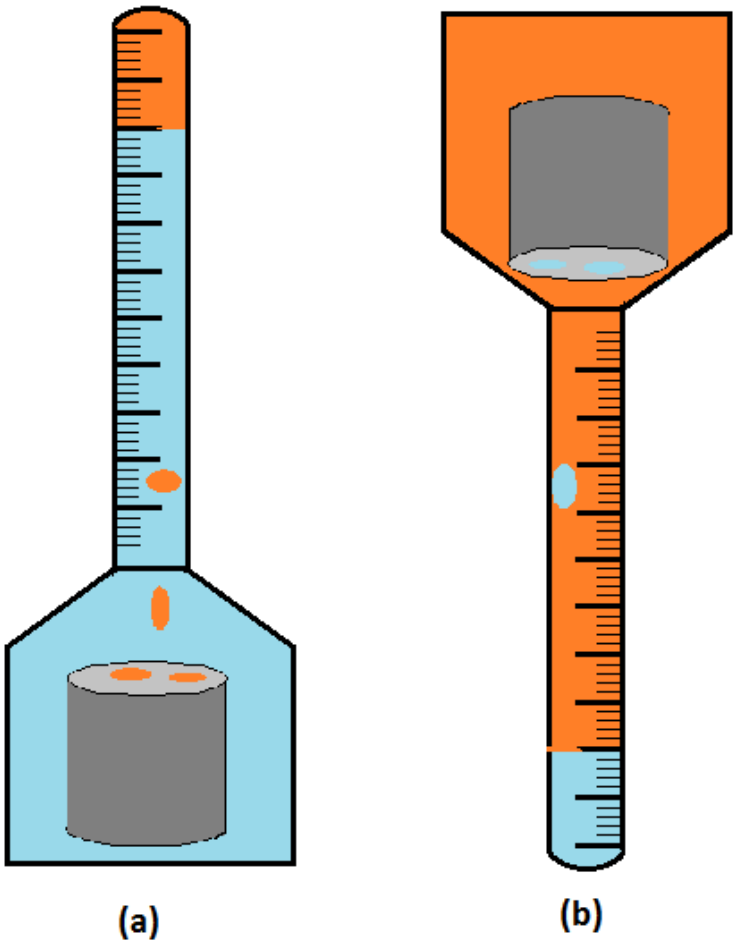

Figure 22: Imbibition cells filled with brine(a) and n-decane(b).

4.3.6 Fracturing of Cores

To study the oil recovery from fractured cores by foam and CO_2 injection, some cores were fractured. A band-saw was used to make a clean cut through the diameter of the core along the cylinder axis. The blade-thickness was 3mm and produced a smooth fracture with almost no roughness at the surface. The initial water saturation and porosity of the rock was assumed to not to change. The cores were either fully saturated with n-decane or with an irreducible water saturation when fractured.

The new pore volume, PV_{frac}, is given by

$$PV_{frac} = PV - (0.3 \cdot D \cdot L \cdot \Phi) \quad (20)$$

where PV is the pore volume without fracture, 0.3 is the width of the blade on the band saw [cm], D is the diameter of the core, L is the length of the core and ϕ is the porosity of the rock.

A spacer was used to fill the fracture and to keep the fracture open at all times. Spacer dimensions were 7.0 cm length, 4.9cm height and 0.1cm thickness and contain 2 open spaces which have a total volume of 2.46ml. The same spacer is used in every fractured rock to make the experiments as consistent as possible.

4.3.7 Fracture Permeability Measurement

The fracture permeability was measured with Darcys law using n-decane only. This was done in order to prevent disturbing the existing fluid saturation in the cores.

5 Experimental Design

5.1 Material balance experiments with liquid CO_2 injection

The experimental setup for the material balance experiments for liquid CO_2 injection was done in University of Bergen and is shown in Figure 23. The experiments were done in room temperature (20°C) and a line pressure at about 95 bar.

Equipment used:

- Hassler core holder(2 inches diameter)
- Quizix QX pump and a handpump for the confinement pressure
- Swagelok tubing, fittings and valves
- Validyne DP15 differential pressure
- Safety pressure regulator
- Back pressure regulator (BPR)
- Web-camera to take picture of the graded cylinder in a given frequency

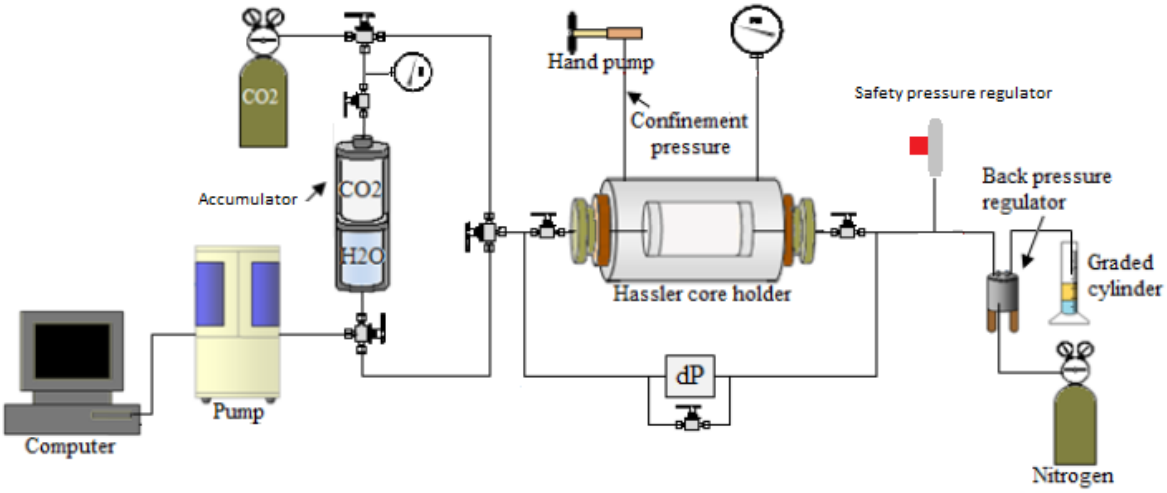

Figure 23: Schematically illustration of the experimental setup for material balance experiments with liquid CO_2 injection. Modified from (Haugen, 2012).

After the initial preparation described in chapter 4.3, the cores were wrapped in aluminum foil to prevent contact between CO_2 and the rubber sleeve inside of the Hassler core holder Figure 24. CO_2 will react with the residual water and create carbonic acid, which can destroy the rubber sleeve and o-rings in the system.

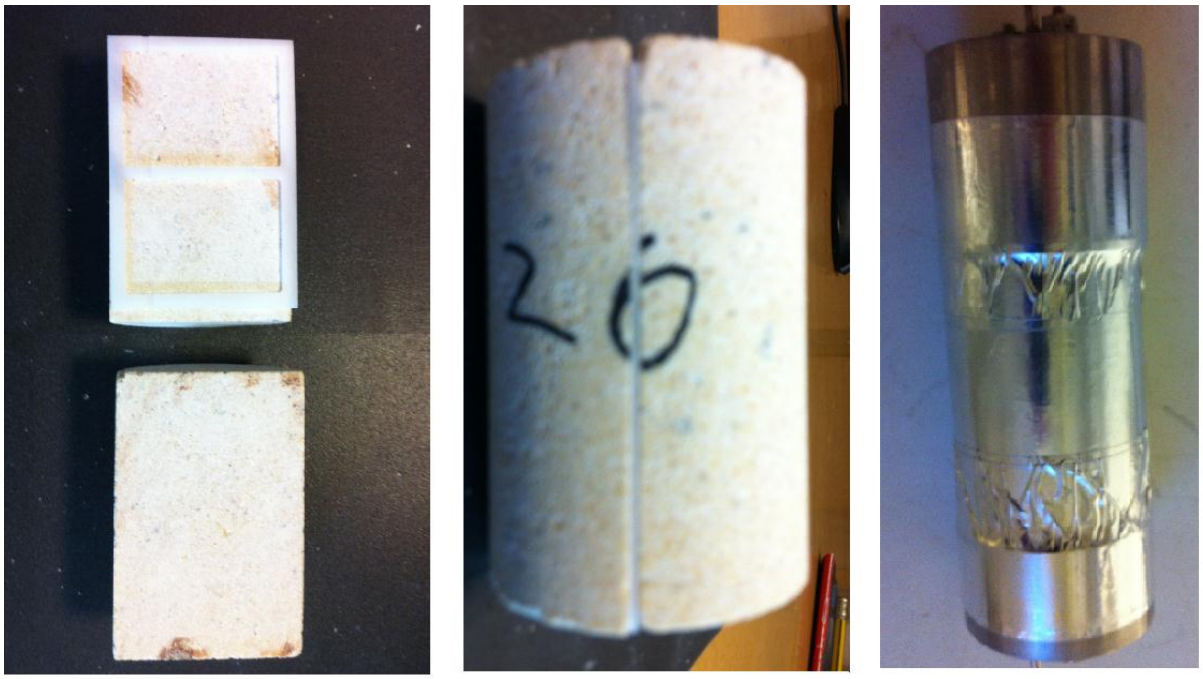

Figure 24: Pictures of a fractured core with spacer. The third picture is the core and the end-points wrapped in aluminum.

The end-piece of the inlet side was filled with n-Decane before connected to the core, to prevent air flowing inside the core. After the end-pieces were put inside the core holder the confinement pressure was increased and n-Decane was injected through the system at a low pressure, about 1bar. The BPR was then gradually increased to 90bar, and the system was pressurized with n-Decane the injected oil was observed downstream of the BPR. The confinement pressure was regulated to always be 10bar above the line pressure. The pump was then set at constant pressure while the system was checked for leaks.

The CO_2 accumulator was pressurized to the line pressure. The CO_2 injection started by opening the first and second valve between the pump and the core holder, and injecting water in the bottom of the accumulator, at the rate of 4mL/h. The oil production at the outlet, downstream of the BPR, was measured by taking picture with a web-camera every 0.5 -1 hour.

The dead-volume of the system is the end piece of inlet side, the whole outlet side and the volume needed to pressurize the system from 1bar to 90bar. The safety pressure regulator and the differential pressure was filled with water instead of oil to be sure that he CO_2 would not mix with it and thereby increase the dead volume.

In one of the material balance experiments, a “huff and puff”-injection with CO_2 was done. This type of injection was done by injecting CO_2 for an hour and then stops it for 2 hours. And this was done over and over again, until endpoint was reached. During the night the pump was off. The total experiment took 14 days.

5.2 Material balance experiments with CO_2-Foam injection

The experimental setup for the material balance foam experiments is shown in Figure 25, and was performed at Texas A&M University. The experiments were performed at 20 °C and 90bar, injecting CO_2 simultaneously with surfactant in order to create foam. Before entering the core, CO_2 and surfactant were co-injected through a glass bead packed foam generator. As a result the foam was formed upon entering the core.

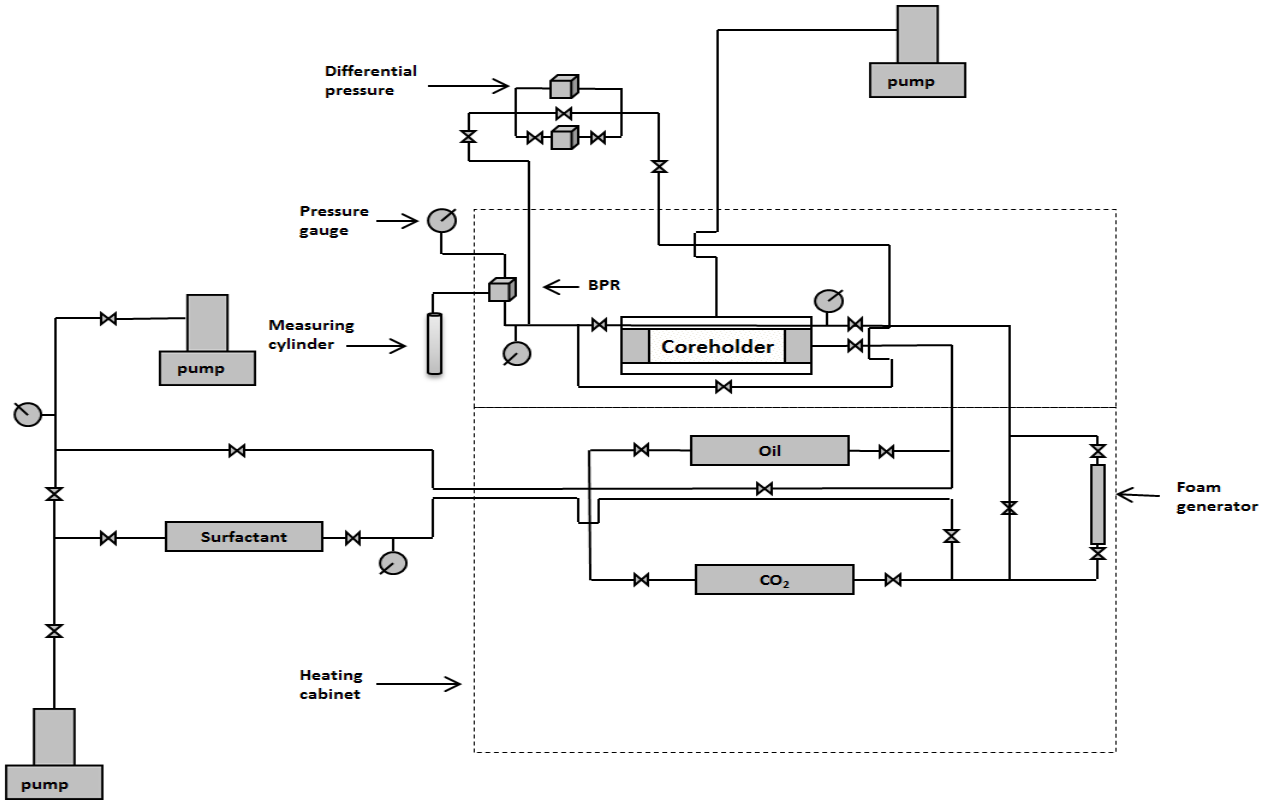

Figure 25. Schematic illustration of experimental setup for the Foam-experiments at Texas A&M University. (Langlo, 2013)

Equipment used:

- 3 ISCO pumps
- Bi-axial (hydrostatic) Core holder with a Isco pump controlling the confinement pressure
- 3 Accumulators
- Validyne DP15 differential pressure
- Swagelok tubing, fittings and valves
- Web camera for taking pictures of the production and differential pressure at regular intervals
- Back pressure regulator supported with nitrogen
- Foam generator (10 cm ¼" Swagelok tubing filled with glass beads)
- Pressure gauges

6 Results

6.1 Porosity and permeability

Basic properties of the cores were measured during core analysis and are presented in Table 2. The average porosity and permeability has been measured on three different rock types, Edward limestone, Portland chalk and Stevens chalk, and only the porosity on sandstone. Core L14, L28 and L33 were used for the material balance experiments for foam injection in Texas A&M University.

The results showed heterogeneous values for the Edwards limestone, with porosity ranging from 17.3%-25.4% and the permeability ranging from 12.5mD-58.7mD. L21 and L22 stands out with a porosity of 17.29% and 17.33%, while the porosity for the rest of the limestones are 21.37%-25.36%. This is presented in Figure 26.

The sandstones, Portland chalks and Stevens chalk core plugs (K7 and K12) showed more homogenous values, with porosity ranging 21.6%-23.3%, 45.0%-47.3% and 49.3%-51.9% respectively. The permeability of the Portland chalks and Stevens chalks ranged 2.8mD-3.5mD and 6.7.mD-6.9mD respectively. Permeability of the sandstones was not measured because it was used to test the systems only.

Table 2: Core identification and properties for the cores used in this thesis

Core	Length [cm]	Diameter [cm]	Pore volume [ml]	Porosity [%]	Permeability K_{matrix} [mD]
L1	7.37	4.96	32.05	22.54	14.93
L2	7.38	4.96	33.52	23.53	30.12
L3	7.58	4.98	31.56	21.37	12.48
L4	7.32	4.96	32.87	23.27	28.56
L5	7.59	4.95	33.76	23.08	22.96
L6	7.36	4.97	33.82	23.69	29.29
L7	6.74	4.96	29.55	22.70	18.52
L8	7.26	4.95	30.81	22.06	17.70
L9	7.59	4.99	33.35	22.46	24.53
L10	7.08	4.96	32.39	23.70	29.57
L11	7.06	4.96	31.37	23.01	21.12
L12	7.64	4.96	33.43	22.63	14.26
L13	8.03	4.95	33.50	21.64	12.49
L14	7.27	4.96	32.84	23.36	28.20
L15	7.35	4.96	32.30	22.75	18.57
L16	7.66	4.95	32.49	22.02	15.00
L17	7.25	5.16	38.40	25.36	51.05
L18	7.12	5.16	35.82	24.08	49.79
L19	7.03	5.16	35.03	23.85	40.17
L20	6.97	5.16	35.88	24.65	55.34
L21	7.29	5.72	30.32	17.33	46.96*
L22	7.34	5.74	30.60	17.29	46.96*
L23	7.13	4.98	28.64	22.32	58.68
L24	7.06	4.97	31.93	23.28	35.23
L25	7.47	4.96	30.65	23.05	28.02
L26	7.29	4.95	32.59	25.16	41.70
L27	7.53	4.96	34.99	24.04	19.88
L28	7.67	4.96	35.67	24.04	19.88
L33	7.05	4.97	34.01	24.89	33.55
S1.5"1	8.60	3.75	21.89	23.09	-
S1.5"2	9.27	3.75	22.77	22.21	-
S1.5"3	8.97	3.75	22.20	22.45	-
S1.5"4	9.13	3.75	23.24	23.05	-
S2.0"1	7.76	5.06	36.33	23.34	-
S2.0"2	9.76	5.07	41.67	21.19	-
S2.0"3	9.41	4.96	39.77	21.86	-
S2.0"4	9.74	5.06	42.19	21.55	-
S2.0"5	9.31	5.05	42.49	22.80	-
K1	8.01	5.07	72.69	44.95	2.82
K2	7.45	4.95	66.57	46.45	-
K3	8.00	5.07	74.60	46.24	2.91
K4	7.79	4.94	70.85	47.34	3.51
K5	7.63	4.95	67.72	46.16	2.89
K6	7.25	4.95	65.60	47.09	3.09
K7	7.58	5.07	75.27	49.26	6.73
K8	7.66	4.98	68.97	46.24	3.09
K9	7.35	4.95	66.76	47.17	3.11
K10	7.28	4.95	64.78	46.26	2.89
K11	7.50	4.94	67.75	47.09	3.23

The permeability of L21 and L22 were not measured, but was put as the average of L23 and L24 since these 4 limestone was drilled out from the same rock.

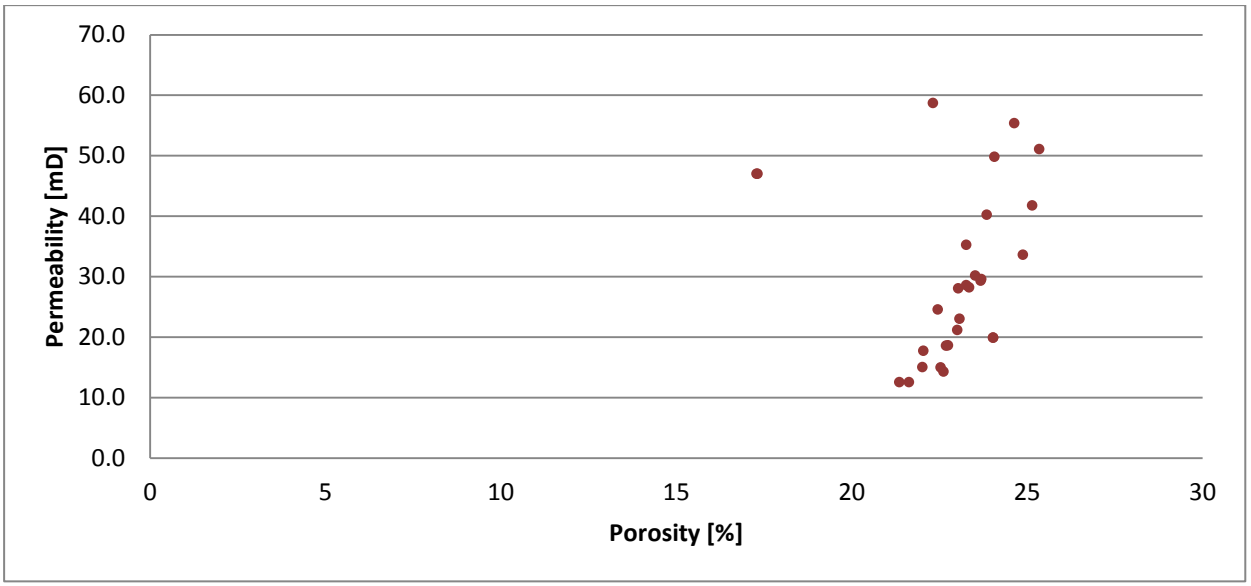

Figure 26: Permeability vs. porosity for the Edward limestone cores. The porosity of L21 and L22

6.2 Wettability measurement

The aging of the cores was performed to obtain a more oil-wet wettability and was calculated by using Equation (15). All of the cores were aged for 90 hours with the same aging procedure. The results are showed in Table 3

Table 3: Aging time, aging method and wettability of the aged cores

Core	I_w	I_o	Amott-Harvey index
L4	0.00	0.02	-0.02
L14	0.00	0.06	-0.06
L2	0.10	0.00	0.10
L7	0.00	0.04	-0.04
L15	0.00	0.10	-0.10
L1	0.00	0.02	-0.02
L16	0.00	0.03	-0.03

The Amott-Harvey index ranged between -0.10 and +0.10 which means they have a neutral wettability. Core L2 is the only core that imbibed water and not oil of the seven cores which means it has a more water-wet preference than the others.

6.3 MMP Simulations

Minimum miscibility pressure (MMP) for a CO_2 and n-Decane system were obtained using WinProp (2012) PVT simulator by Computer Modeling Group (CMG). The MCM (multiple contact miscibility) option was used to calculate the first contact miscibility for the system. This is done with various temperatures and presented in Figure 27.

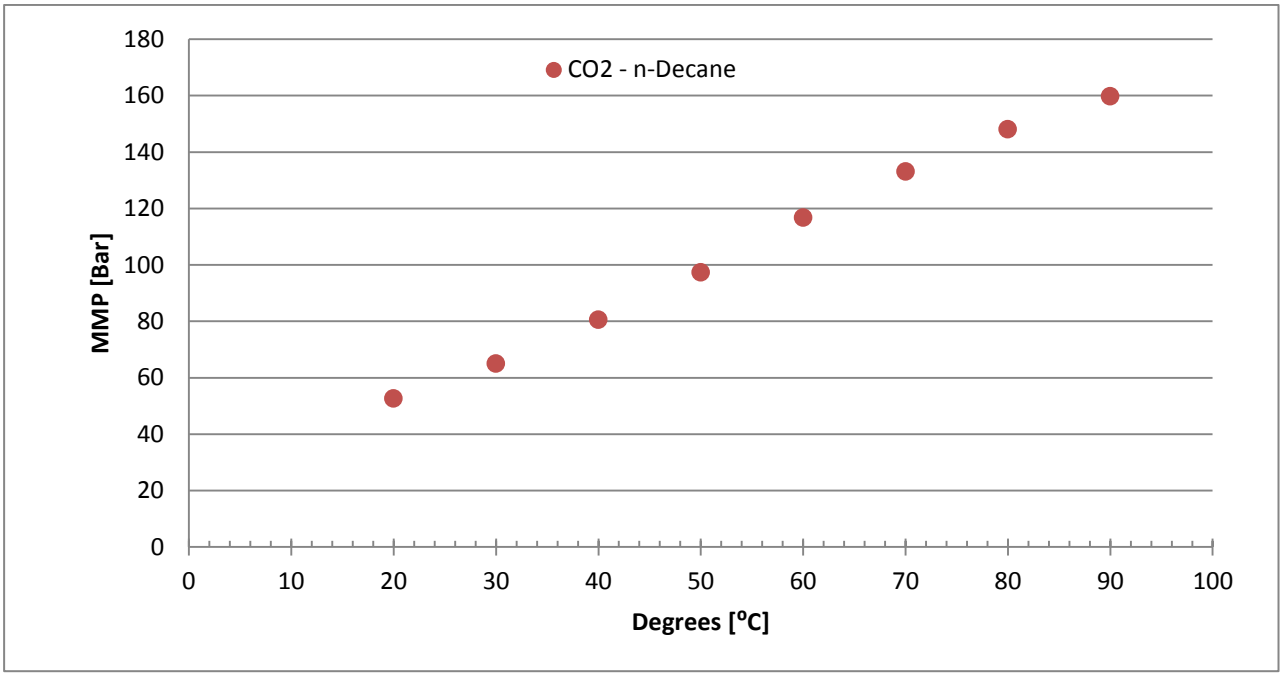

Figure 27: MMP vs. temperature for a CO_2 and n-decane system. MMP values generated from WinProp PVT simulator from CMG.

Based on these results it was decided that the experiments should be done with 20 °C and at least 85bar to ensure miscible displacement.

6.4 CO_2 injection in strongly water-wet cores

This chapter describes the results during CO_2 injection for EOR in 11 limestone cores and 1 sandstone listed in Table 4. Six core plugs were 100% oil saturated, 4 whole (3 limestone and sandstone core S2”1) and 2 fractured. Six cores had irreducible water saturation, where 3 were whole and 3 were fractured.

Table 4: Experimental conditions and results from experiments with CO_2 injection in strongly water-wet (SWW) cores.

Core	Description	Injection	State	S_{wi}	K_{matrix} [mD]	$K_{fracture}$ [mD]	Line Pressure [bar]	S_{or}	RF [%OOIP]
S2”1	100% oil	CO_2	Whole	0,00	1000	-	85	0.08	92
L17	100% oil	CO_2	Whole	0.00	51.0	-	92	0.00	100
L19	100% oil	CO_2	Whole	0.00	40.2	-	91	0.05	96
L20	100% oil	CO_2	Whole	0.00	55.3	-	94	0.00	100
L21	100% oil	CO_2	Fractured	0.00	47.0	1080	92	0.07	93
L22	100% oil	CO_2	Fractured	0.00	47.0	1080*	97	0.08	92
L6	S_{wi}	CO_2	Whole	0.14	29.3	-	91	0.11	87
L9	S_{wi}	CO_2	Whole	0.23	24.5	-	86	0.07	91
L10	S_{wi}	CO_2	Whole	0.20	29.6	-	80	0.06	92
L23	S_{wi}	CO_2	Fractured	0.13	58.7	1342	97	0.22	75
L26	S_{wi}	CO_2	Fractured	0.23	41.7	1318	91	0.12**	84
L25	S_{wi} Huff and puff	CO_2	Fractured	0.26	28.0	1366	98	0.05	93

* The fracture permeability of L22 was not measured, but assumed to be equal to L21 because the same spacer was used

** Did not reach the endpoint, which means that S_{or} is lower.

The following subchapters describe the CO_2 injection of 100% saturated core and cores with S_{wi}.

6.4.1 CO_2 injection in sandstone - 100% oil saturated

Figure 28 shows the development of the average oil saturation and recovery factor versus pore volume for sandstone S2”1 during CO_2 injection. The production was linear until CO_2 breakthrough after 0.35 PV. With breakthrough the oil production decreased drastically and 6PV was injected until reaching residual oil saturation, S_{or}, at 0.08 and recovery factor at 92 % OOIP.

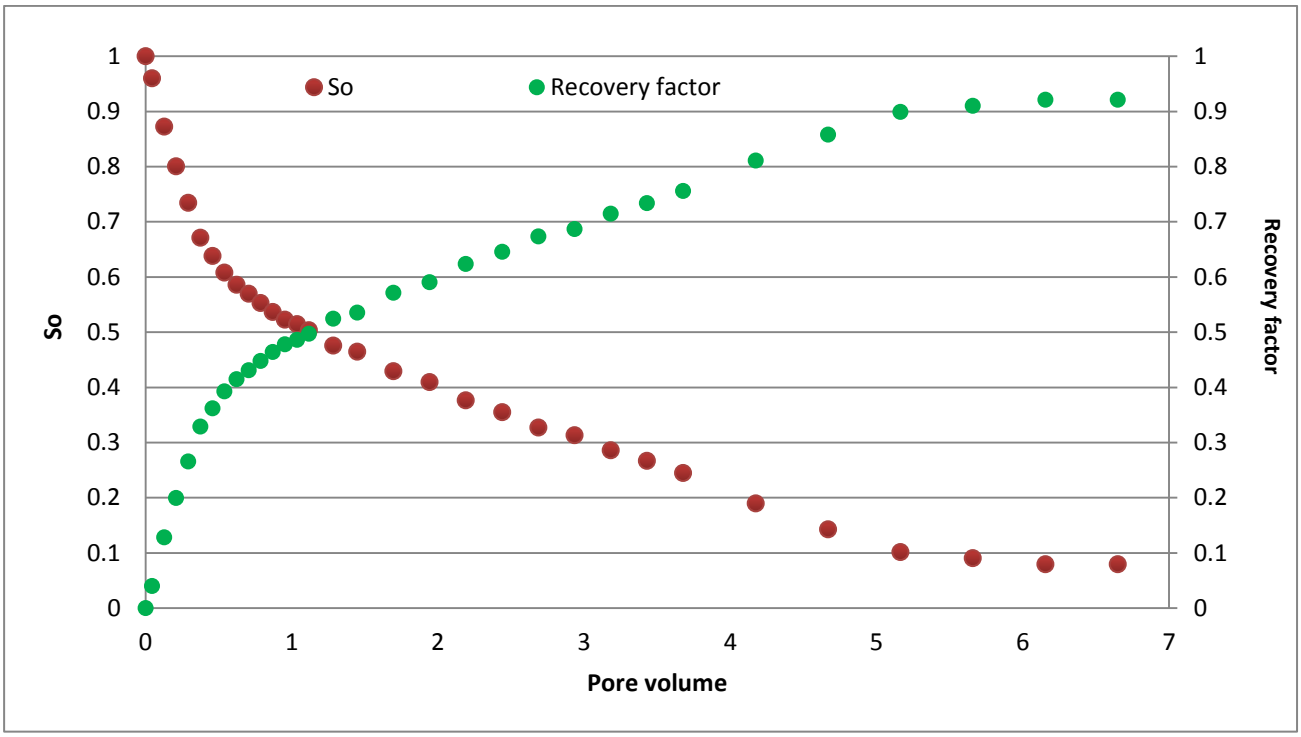

Figure 28: Average oil saturation and recovery factor vs. pore volume CO_2 injected for core S2"1

6.4.2 The influence of fracture on CO_2 EOR in limestone - 100% oil saturated

Figure 29 shows the development of the average oil saturation and recovery factor versus pore volume injected for 3 whole and 2 fractured limestone cores at 100 % oil saturation.

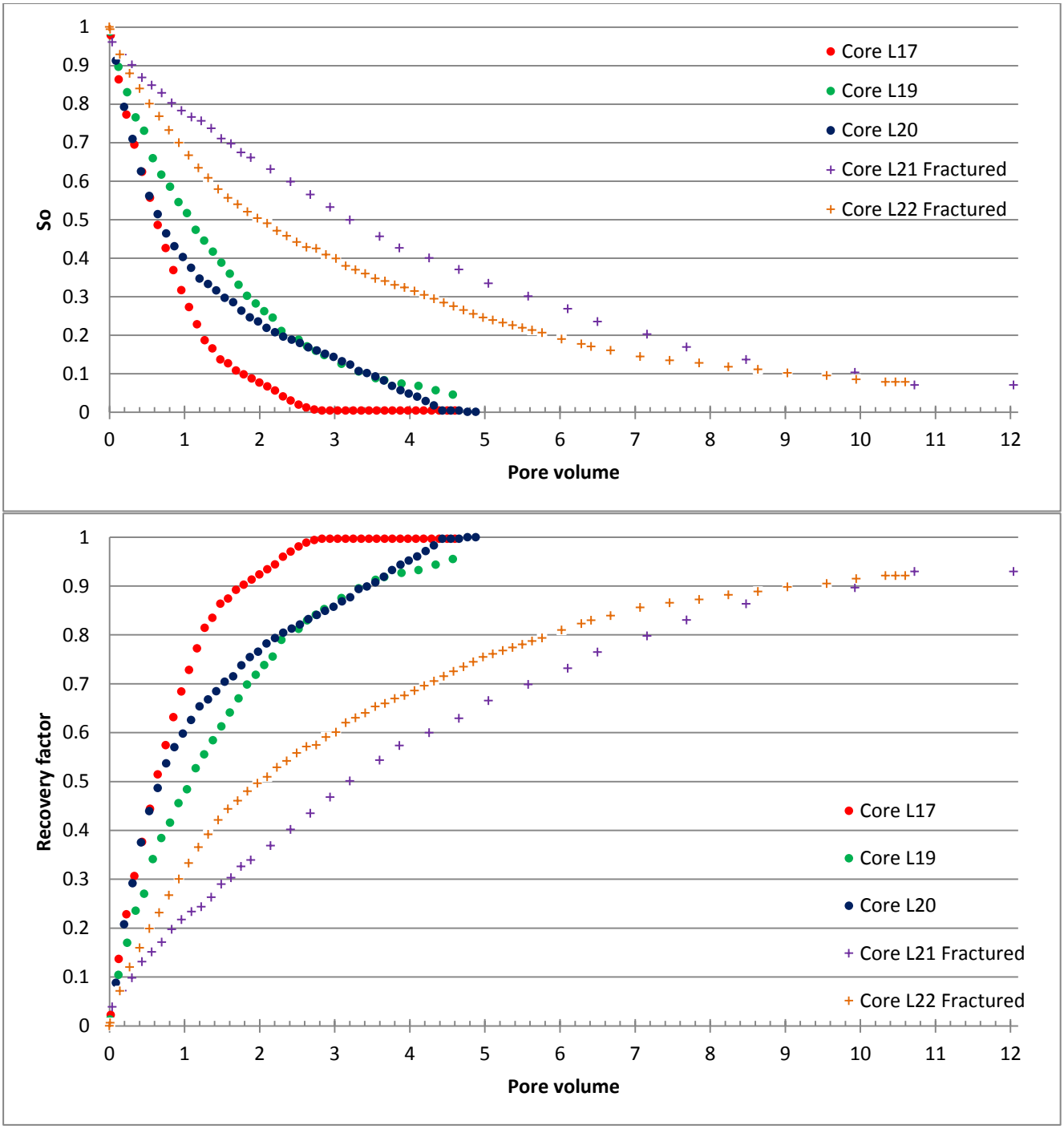

Figure 29: S_o (Top) and Recovery factor (Bottom) vs. pore volume CO_2 injected into 100% oil-saturated limestone cores. 3 Whole and 2 fractured.

Core plug L17 had breakthrough at 0.2 PV CO_2 injected, but the oil production rate remained high, with recovery factor at 70 % after 1 PV of CO_2 injected. The endpoint was reached after 2.8 PV with S_{or} at 0.04 and RF at 100 %.

The confining pressure of L19 decreased rapidly and got close to the line pressure at the start of the experiment, and was not increased until 0.5PV. L19 had therefore a CO_2 breakthrough at 0.1PV and a production rate much lower than L17. The endpoint after 4.6 PV was S_{or} at 0.05 and RF at 96 %.

Core plug L20 had breakthrough at 0.3PV and maintained a high production rate until 0.65 PV. After 2.8 PV, oil production seems to have slightly increased before reaching end-point at 5PV, with S_{or} at 0.00 and RF at 100 %.

Because L21 and L22 were fractured and the fracture was filled with CO_2, breakthrough was not established and CO_2 was produced at very beginning. Since the line pressure of L22 dropped from 91bar to 85bar at 2.6PV, the back pressure regulator was increased to 100bar. The end-point of L21 was reached at 10.7PV with S_{or} at 0.07 and RF at 93 %. The end-point of L22 was reached at 10.4PV with S_{or} at 0.08 and RF at 92 %.

6.4.3 CO_2 EOR for limestone core plugs with irreducible water saturation

Figure 30 shows the development of the average oil saturation and recovery factor versus pore volume injected for 3 whole and 3 fractured limestone cores at irreducible water saturation.

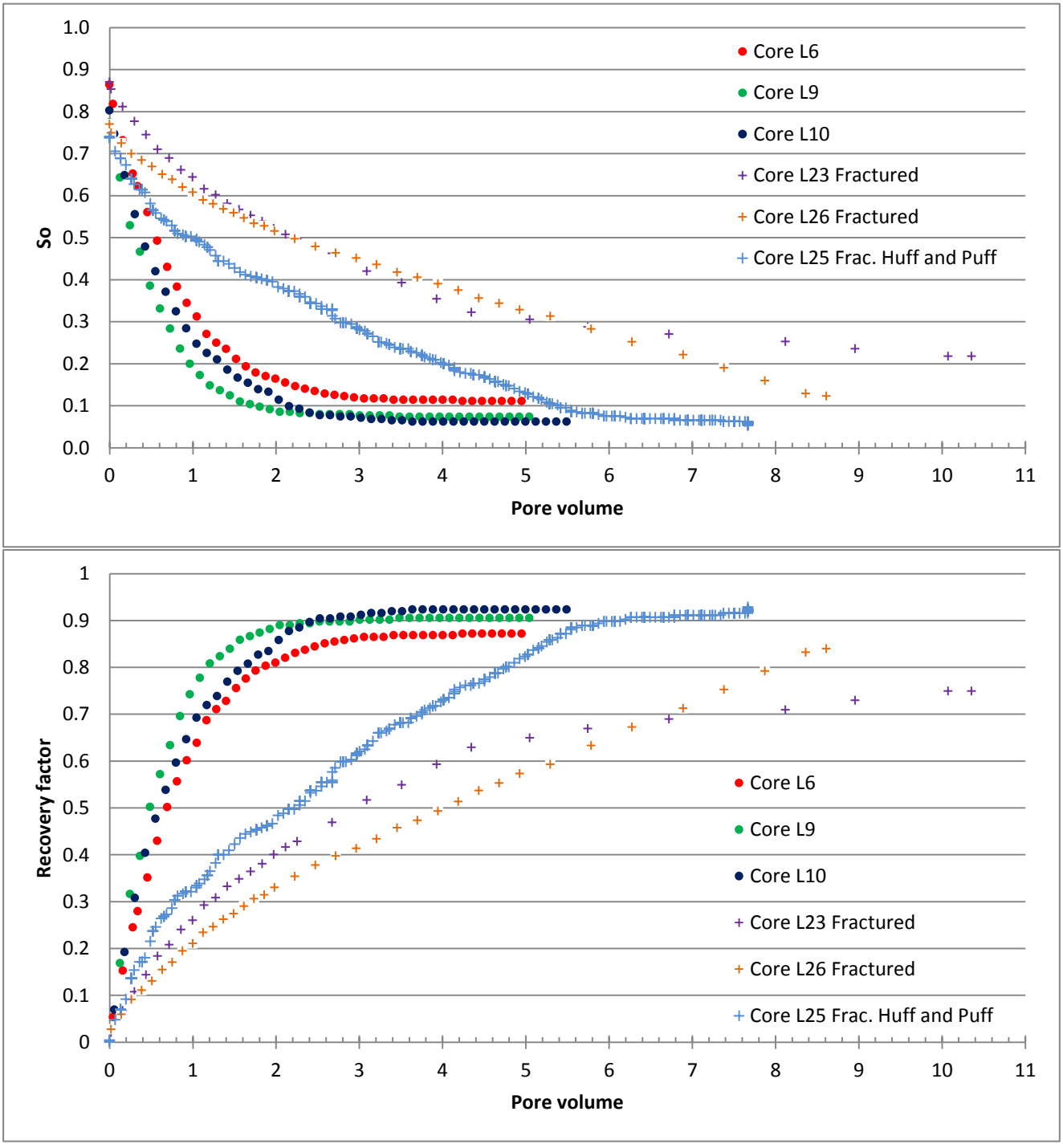

Figure 30: S_o (Top) and Recovery factor (Bottom) vs. pore volume CO_2 injected into limestone cores with irreducible water saturation. Whole, fractured and fracture with a huff and puff-process.

CO_2 injection in whole core plug L6 was stopped for 48 hours after 0.35 PV injected without an observable effect on the rate of recovery. One might expect an increase in recovery because core is left for 48 hours to diffuse, but because breakthrough has not taken place, the direction of diffusion has been controlled by the concentration gradient. The highest CO_2 concentration is at the inlet of the core, unlike a fractured core where the highest concentration will be in the middle. The end-point of L6 was reached at 4.2PV with S_{or} at 0.11 and RF at 87 %.

Breakthrough of CO_2 at the outlet for cores L9 and L10 was observed after 0.49PV and 0.55PV, respectively. They have a similar curve as L6, even though L6 had an incubation time. The line pressure of L10 and the BPR decreased from 85bar to 75bar at 2.9PV, and the BPR was thereby increased to 85bar. The end-point of L9 was reached at 3.5PV with S_{or} at 0.07 and RF at 91 %. The end-point of L10 was reached at 3.6PV with S_{or} at 0.06 and RF at 92.3 %.

The fractured cores L23 and L26 did not have steep curves as the whole cores, as expected. The production curve for L23 was almost linear after 1.3PV and did not reach final residual S_{or}. The end-point of L23 was at 8.6PV with S_o at 0.12 and RF at 84 %. The production curve for L26 has the same trend as the whole cores, but with lower production rate. The end-point of L26 was reached at 10.1PV with S_{or} at 0.22 and RF at 75 %.

The huff and puff experiment for core L25 showed a higher production rate per pore volume compared to continuous CO_2 injection in fractured cores(L23 and L26), but lower rate than the whole cores (L6, L9 and L10). The production curve looks almost like a staircase with a steep part and an almost flat part. The end-point of L25 was reached at 7.7PV with S_{or} at 0.05 and RF at 93 %.

6.5 CO_2 injection in neutral-wet cores

This chapter shows the average oil saturation and recovery factor vs. time during CO_2 injection in 4 neutral-wet cores with irreducible water saturation present in the pore space at the start of the injection. Four CO_2 injections were performed in 3 whole and 1 fractured cores. Table 5 lists the final recovery and residual oil saturation, and Figure 31 shows the development in average oil saturation and recovery for the cores.

Table 5: Experimental conditions and results from experiments with CO_2 injection for neutral-wet cores.

Core	Description	Injection	State	S_{wi}	K_{matrix} [mD]	$K_{fracture}$ [mD]	S_{or}	RF [%OOIP]
L7	S_{wi}	CO_2	Whole	0.33	18.5	-	0.00	100
L4	S_{wi}	CO_2	Whole	0.39	28.6	-	0.00	100
L16	S_{wi}	CO_2	Whole	0.33	15.0	-	0.15	77
L2	S_{wi}	CO_2	Fractured	0.32	30.1	1255	0.28	59

The water saturation to the neutral wet-cores is 0.10-0.26 higher than the strongly water-wet cores.

Core plug L7 had a linear production until 0.6PV, when a leak in the confining pressure reduced pressure to the line pressure and thereby led the CO_2 flow around the core. The confining pressure was reestablished after 1.3PV and the production rate increased. The end-point of L7 was reached at 4.8PV with S_{or} at 0.00 and RF at 100 %.

L4 had breakthrough at 0.4PV and the curves have almost the same shape as L7 at the start and end of the CO_2 injection. The end-point of L4 was reached at 4.2PV with S_{or} at 0.00 and RF at 100.0 %.

CO_2 injection in core plug L16 was not completed due to the safety pressure was triggered and a very early breakthrough which led to the low production rate. The curves to L16 distinguish itself from L4 and L7 with a low production rate and an early breakthrough at 0.1PV. The end-point of L16 was reached at 4.9PV with S_{or} at 0.15 and RF at 77 %.

L2 is the only fractured, neutral-wet core with CO_2 injection. The oil production is low and does not reach end-point after 17.2PV, with residual oil saturation at 0.28. The oil recovery factor is 59 % which is the lowest recovery factor of all the experiments. Even though this core is the only fractured neutral wet core it will not be discussed in section 7, because the recovery factor and production rate is much lower than expected, because Malin Haugen achieved 81%-97% recovery for both whole and fractured Portland chalks that were aged.

Core L7 and L16 will not be discussed in the discussion chapter since L7 had a problem with the confining pressure, and clearly changed the development in average oil saturation and recovery.

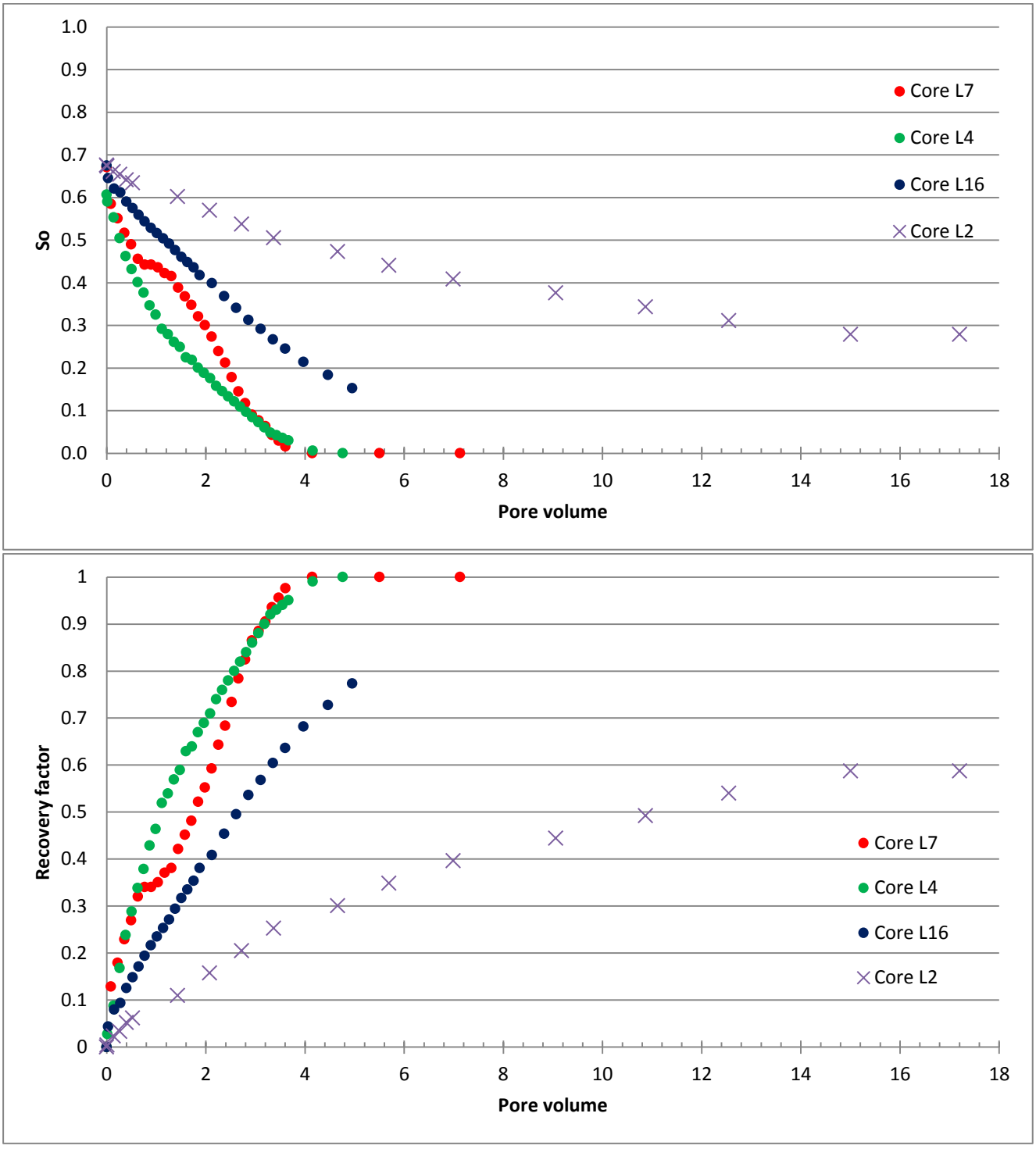

Figure 31: S_o (Top) and Recovery factor (Bottom) vs. pore volume CO_2 injected into whole and fractured neutral-wet cores.

6.6 Foam injection

This chapter shows the average oil saturation and recovery factor vs. time during foam injection in 2 strongly water-wet cores and 1 neutral-wet core with irreducible water saturation present in the pore space at the start of the injection, where all 3 cores are whole. Table 6 lists the final recovery, and Figure 32 shows the development in average oil saturation and recovery for the cores.

Table 6: Experimental conditions and results from experiments with foam injection.

Core	Description	Injection	State	S_{wi}	K_{matrix} [mD]	S_{or}	RF [%OOIP]
L28	SWW, S_{wi}	Foam	Whole	0.24	19.9	0.27	65
L33	SWW, S_{wi}	Foam	Whole	0.29	33.5	0.06	91
L14	NW, S_{wi}	Foam	Whole	0.29	28.2	0.01	98

Oil production from core plug L28 was linear until 0.26PV, which seems to be the breakthrough of CO_2. After 0.5PV the oil production rate decreases drastically compared to L33 and L14. Surfactant solution was observed at the outlet at 2PV injected. The end-point of L28 was reached at 2.7PV with S_{or} at 0.27 and RF at 65 %. The differential pressure varies between 120 and 160mbar.

Breakthrough of CO_2 for core plug L33 was observed at 0.39PV, but a high production rate was maintained after breakthrough. The surfactant was observed at the outlet at 1.4PV injected. The end-point of L33 was reached at 2.6PV with S_{or} at 0.06 and RF at 91 %. The differential pressure varies between 60 and 140mbar.

L14 reached breakthrough at 0.30PV, and the curves had the same trend as L33. The end-point of L14 was reached at 4.2PV with S_{or} at 0.01 and RF at 98 %. The differential pressure is much lower than L28 and L33 and varies between 2 and 6mbar.

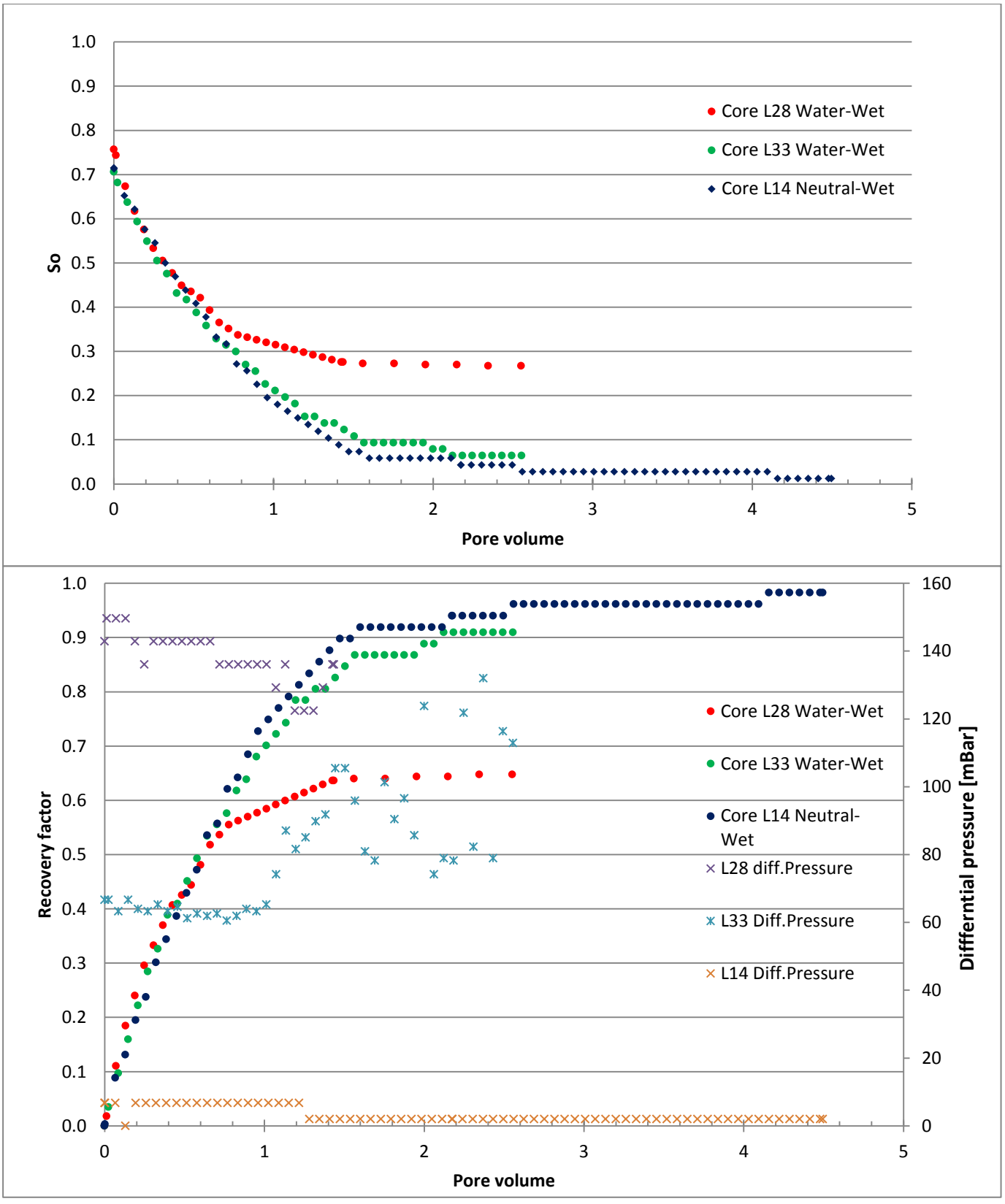

Figure 32: S_o (Top), Recovery factor and differential pressure (Bottom) vs. pore volume foam injected into water-wet and neutral-wet cores. The cores are not fractured.

6.7 Simulation

The experimental results from L23 and L26 were further investigated in a numerical model using GEM, Builder and WinProp in the CMG (Computer Modeling Group) software. The cores were remodeled as a cube, where the length was 1:1 with the core length, height was 1:1 with the radius of the core and the thickness was 20% of the diameter of the core. The inlet and outlet side of the core were connected to large volumes of CO_2 which would simulate the wells. The fracture was also increased to be sure it always was filled with CO_2.

Figure 33 shows the development in oil saturation for L23, where the fracture is on the right side and the inlet and outlet at the top and bottom. The figure clearly shows the diffusion process, were the two fluids mixes to achieve concentration equilibrium.

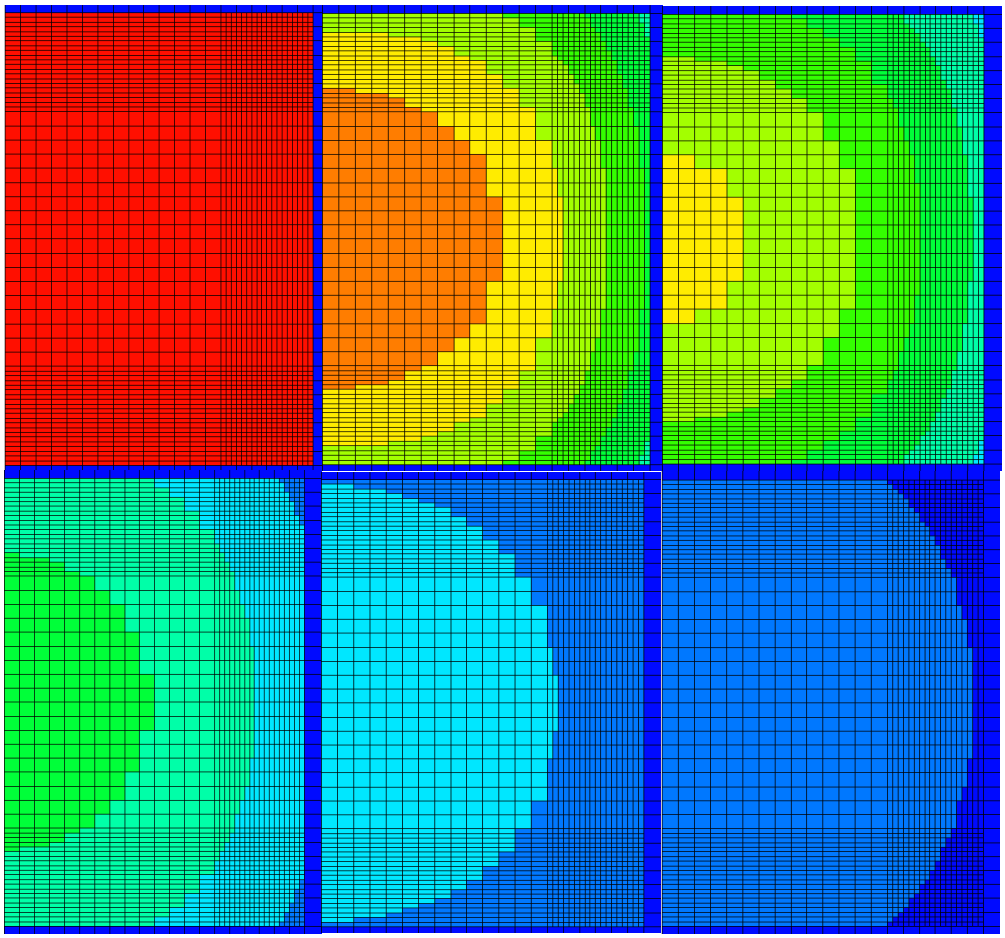

Figure 33: Development in oil saturation in the simulation experiment due to time, where each of slides represents a new time step. Red color denotes high oil saturation while blue color denotes low oil saturation. The fracture is on the right side and the inlet and outlet is at the top and bottom side.

Figure 34 and Figure 35 shows the oil saturation vs. days for the experimental and simulated cores. L26 was simulated as a water-wet core and an oil-wet core but because they showed the exact results it is more likely that some of the data-input was wrong for the oil-wet simulation. Except for the oil-wet simulation, the numerical model successfully reproduced the experimental results for both L23 and L26.

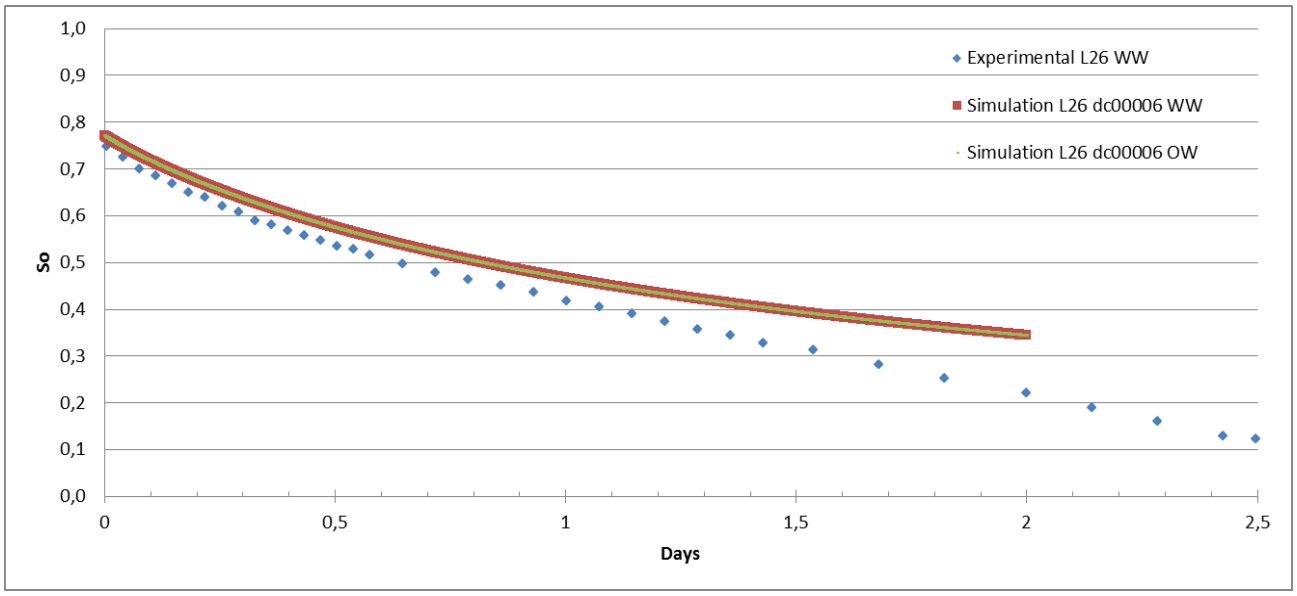

Figure 34: Oil saturation vs. time CO_2 injected for experimental and simulated (water-wet and oil-wet) experiments.

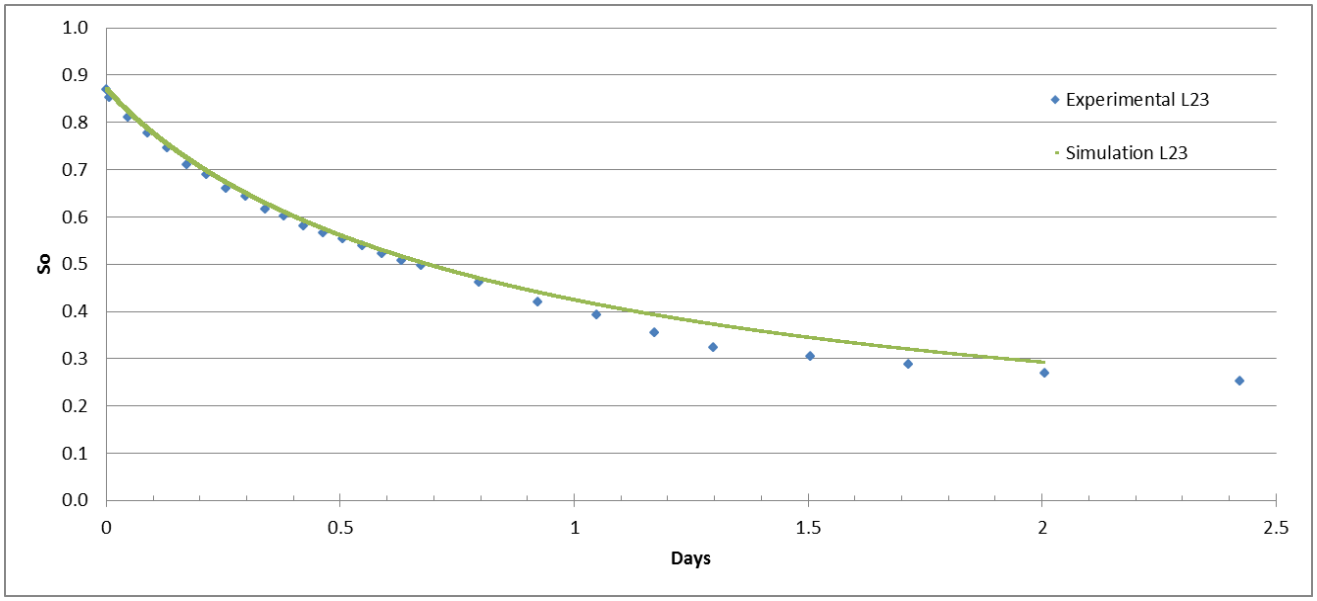

Figure 35: Oil saturation vs. time CO_2 injected for experimental and simulated experiments.

7 Comparison and discussion

In this chapter the results presented in chapter 6 are compared and further discussed. Topics discussed are 1) oil productions during water flooding is compared to CO_2 injection, 2) how the presence of fracture influences oil recovery during CO_2 injection, 3) CO_2-foam injection vs. pure CO_2 – injection and 4)how wettability preference of the matrix influence oil recovery.

7.1 Liquid CO_2 EOR

This chapter discusses the liquid CO_2 injection experiments and the influence of fractures and wettability. Table 7 lists the average total oil recovery, R_f, and average PV injected for each CO_2 experiments.

Table 7: The final average recovery factor for each of the CO_2 experiments

Initial fluid saturation	Whole/Fracture	Wettability	Average Pore Volume Injected	Average Recovery Factor [% OOIP]
100% oil saturated	Whole	SWW	4.7	98
	Fracture	SWW	10.5	93
S_{wi}	Whole	SWW	5.0	90
		NW	4.5	100
	Fracture	SWW	9.0	84
		NW	17.2	59

7.1.1 Water vs. liquid CO_2 injection

Table 7 shows that CO_2 as a secondary injection has a high final recovery factor overall, with the majority of injections in whole cores producing more than 90 % OOIP on average. Fractured core plug with irreducible water saturation exhibited lower average recovery factors with 59 and 84 % OOIP for neutral and water-wet cores respectively.

Compared to CO_2 injection at miscible conditions, the injection of water is less effective. During water injection on 7 limestone core plugs, where 5 core plugs was fractured, the final recovery ranged between 18% - 50% with an average of 30% - (Svenningsen, 2011). The whole core plugs reached end-point at 2 PV and the fracture after 10PV.

Water injection has a linear production curve until breakthrough is reached. If the core plug is water-wet a snap-off event will occur in the pore throats due to strong capillary forces leading to immobile trapped inside the cores by capillary forces and the oil production will stop immediately after water breakthrough. For oil-wet cores, the water will pass through the largest pores and oil trapped in the smallest pores and as a continuous film on the rock surface. After breakthrough oil may still be produced, and the oil phase will be mobile at lower oil saturations compared to water-wet media.

With a miscible displacement as CO_2 injection, the injected fluid will mix with the oil that it contacts, and thereby mobilize it. The disadvantages of CO_2 injection is the mobility ratio between the CO_2 and the oil it displace and gravity segregation as mentioned in chapter 2.2. These disadvantages will be negligible when injecting 4-10PV into core plugs, since CO_2 would have enough time to mix with the oil due to diffusion.

7.1.2 Fracture vs. whole core plugs for CO_2 injection

This subchapter discusses oil recovery vs. time during CO_2 injection in fractured and whole cores. Table 7 lists the average recovery factor for whole and fractured core plugs. As discussed in chapter 7.1.1, CO_2 injection has a high recovery factor for both fractured and whole core plugs. The main difference between the results is the amount of PV injected. Whole cores reached end-point after 4.5 – 5.0 PV CO_2 injected, while the fractured cores reached end-point at 9.0-17.2 PV injected.

Most of the CO_2 injected in fractured core plug flows through the spacer in the fracture, because the fracture permeability is more than 300 times higher the matrix permeability. The oil production in fractured core plug is not driven by viscous displacement but mainly diffusion. Diffusion is as mentioned in section 1.10, a process which leads to equilibrium in the concentration distribution, which means that CO_2 in the fraction will slowly flow into the matrix and the oil into the fracture and thereby produce.

A visualization of CO_2 diffusion into the core plug matrix from the fracture is shown in Figure 36 where the development in oil saturation across a vertical slice in the center of the core may be observed. At 0.00 PV injected, the oil was uniformly spread across the core. At 0.17 PV injected, CO_2 entered the whole fracture and reduced the oil saturation to 50%. Between 0.17 PV and 0.34 PV the oil saturation near the fracture decreased due to diffusion, and after 1.21 PV injected the CO_2 had spread through the whole slice. The concentration gradient is perpendicular to the fracture, which means the oil saturation is low near the fracture and high furthest from the fracture.

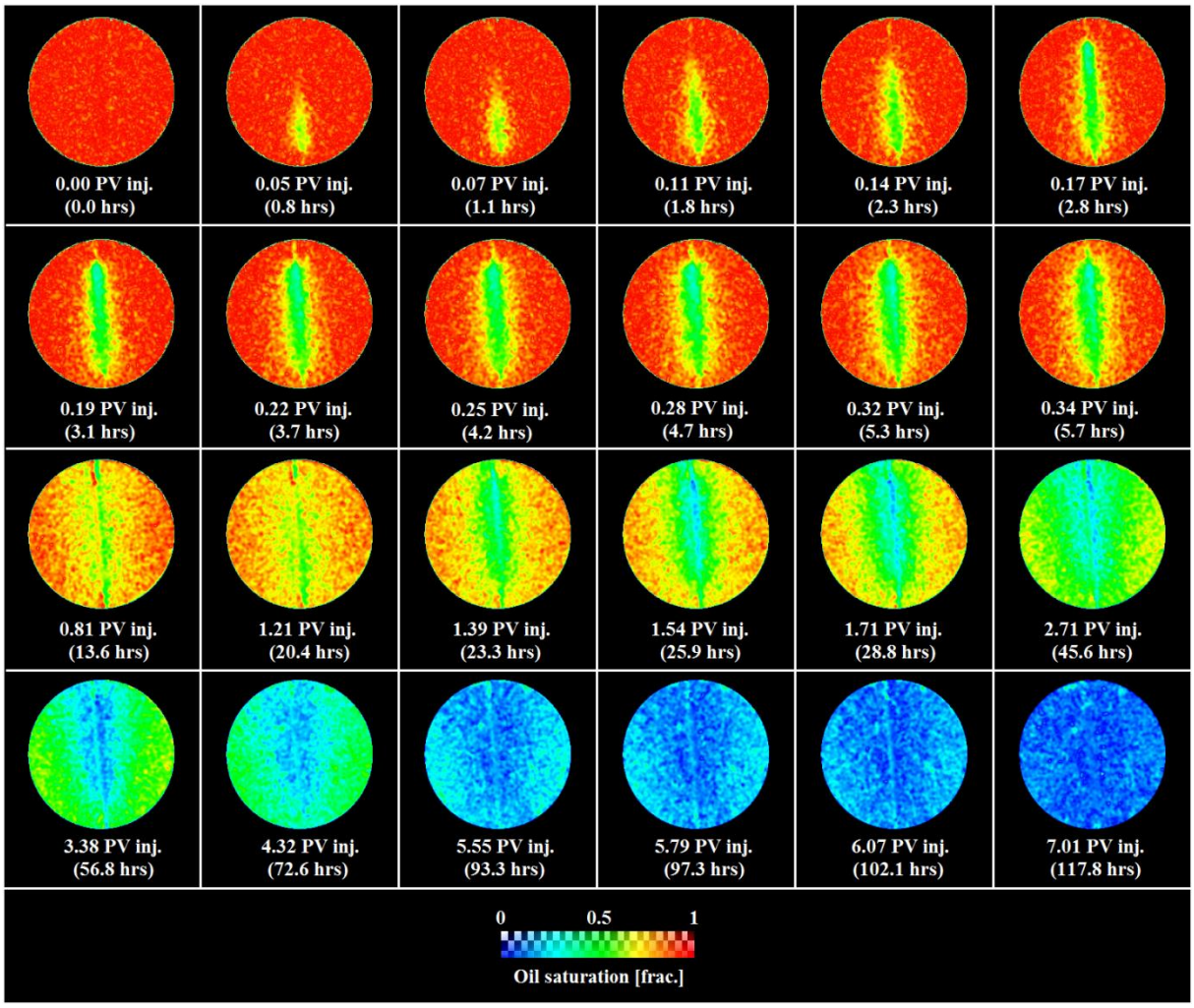

Figure 36: Development in oil saturation in the CO_2 injection experiment across a digital vertical slice in the center of the core. Each slice represents a new time step. Red color denotes high oil saturation while blue color denotes low oil saturation. (Baird, 2013)

Comparing the 100 % saturated cores with the S_{wi} cores, it seems that the irreducible water affect the oil recovery negatively with a lower production rate final recovery. Because CO_2-injection in fractured cores is diffusion driven, water shielding could prevent some oil to mix with the injected CO_2.

The Huff and Puff experiment, L25, increased the recovered oil per volume CO_2 injected compared to pure, continuous CO_2 injection. The experiment took 14 days to reach the end-point, which was the longest experiment in this thesis, but showed that injection with incubation time increased oil production per pore volume CO_2 injected. The oil production rate also varied and was high right after the incubation time and low before the incubation time which indicates that there is a diffusion-process in the core-plug that enhance the recovery.

The benefits of a Huff and Puff injection is the decrease in the volume of CO_2 injected, which is good because CO_2 is expensive. The disadvantages of Huff and Puff are the amount of time it takes to produce. Every experiment with fracture reached end-point before 4 days, whereas the huff and puff used 14 days.

7.1.3 The effect of wettability with CO_2-injection

This sub chapter discusses the effect of wettability with CO_2- injection into whole core plugs. Figure 37 compares the recovery factor for 3 whole water-wet and 1 neutral-wet cores.

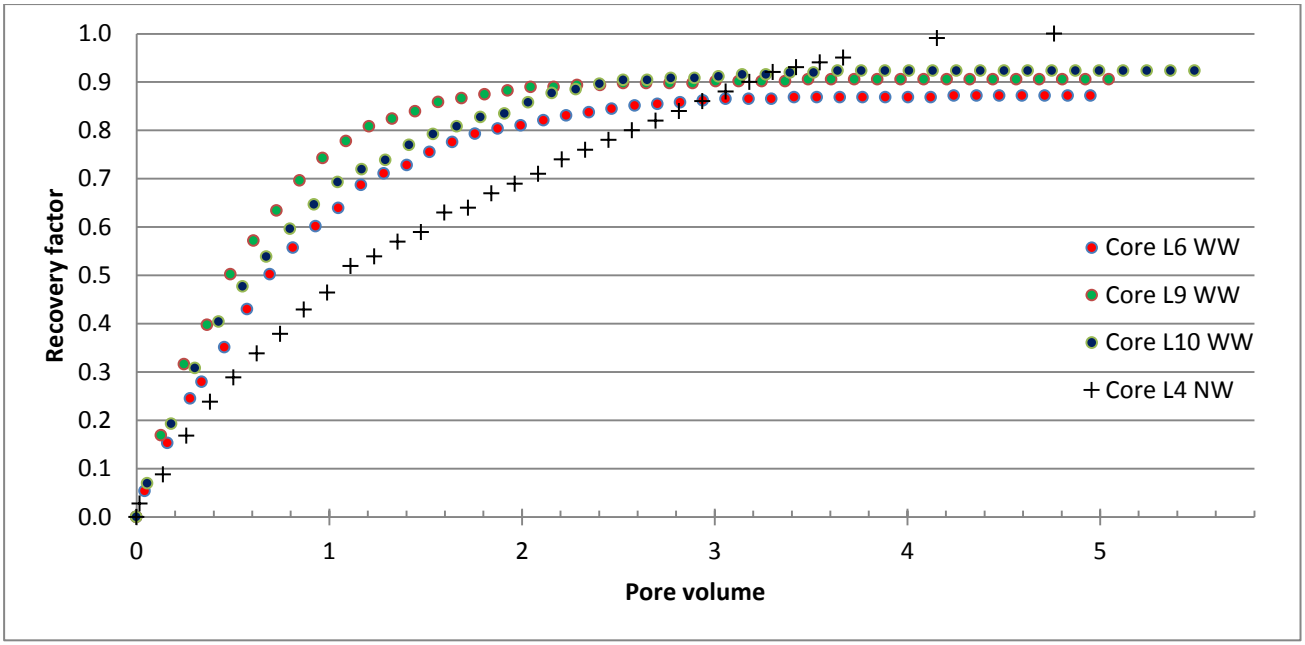

Figure 37: Recovery factor vs. pore volume CO_2 injected into whole core plugs for both water-wet and neutral-wet cores.

For the whole cores, the neutral-wet L4 reached its end-point slower than the water-wet cores and needed an additional 1.3PV injected. Nevertheless, a higher final recovery was observed. The production rate for L4 was lower than the water-wet cores before 2PV injected, which was the end of the transient period for the water-wet cores. The low production rate observed in core L4 could also be a result of the high irreducible water saturation, 39%. Water would then decrease the contact between the oil and the CO_2, which would make the displacement slower. The high recovery for the neutral wet core could be

because the oil is more connected with neutral-wet rocks, which means the miscibility displacement will have a higher effect.

7.2 Foam EOR

This chapter discusses fracture vs. whole core plugs for CO_2-foam injection and compares CO_2 and CO_2-foam injection with different wettabilities. Table 8 lists the final recovery, irreducible water saturation and the initial conditions for 8 foam experiments, where the 3 whole core plugs are the results from this thesis and the 5 fractured cores from Anders Christophersens thesis (EDW16, EDW33, EDW6, EDW32 and EDW39)(Cristophersen, 2012). All of the 5 reference cores are fractured, where 2 are strongly-wet, 1 is neutral-wet and 2 are oil-wet.

Table 8: The results for each of the CO2-foam experiments and reference data from Anders Christophersen

Core	Description	Injection	State	S_{wi}	K_{matrix} [mD]	$K_{fracture}$ [mD]	S_{or}	RF [%OOIP]
L28	SWW	Foam	Whole	0.24	19.9	-	0.27	65
L33	SWW	Foam	Whole	0.29	33.5	-	0.06	91
L14	NW	Foam	Whole	0.29	28.2	-	0.01	98
EDW16	SWW	Foam	Fractured	0.32	26.4	117	0.24	64
EDW33	SWW	Foam	Fractured	0.19	28.5	261	0.17	78
EDW6	OW	Foam	Fractured	0.06	27.5	1980	0.07	91
EDW32	OW	Foam	Fractured	0.17	21.0	265	0.07	92
EDW39	NW	Foam	Fractured	0.11	12.0	1021	0.16	82

7.2.1 The effect of CO_2-foam injection in whole cores

The three experiments performed with injection of CO_2-foam in whole cores are presented in Figure 38 and Table 8. By adding a surfactant to the CO_2 and create foam, makes the injected fluid more viscous then pure CO_2. The mobility ratio between the injected fluid and the displaced fluid will then be lower and delay breakthrough.

Comparing the CO_2-foam experiments with the pure CO_2 experiments (at S_{wi}), it is no particularly difference in the final recovery. CO_2-foam experiments have a final recovery between 65% and 98%, and the pure CO_2 experiments have a final recovery between 59% and 100%. The CO_2-foam experiments seem to have earlier breakthrough then the CO_2 experiments, which were not expected.

The end-point oil saturation was reached after 2.6-2.7PV for the water-wet cores and 4.2 PV for the neutral-wet core. The differential pressure for the water-wet cores was between 60 and 150mbar, which means that foam has not been destroyed inside the core. The observed fluctuation in the differential pressure is related to the creation and destruction of lamellae. The low differential pressure in the neutral-wet L14 could mean that the foam has been destroyed inside the core-plug. Sanchez and Hazlett mention that oil-wet and neutral wettability reduce the generation of foam, because the mechanism behind the generation of new lamellae prefer water-wet conditions (Sanchez and Hazlett, 1992).

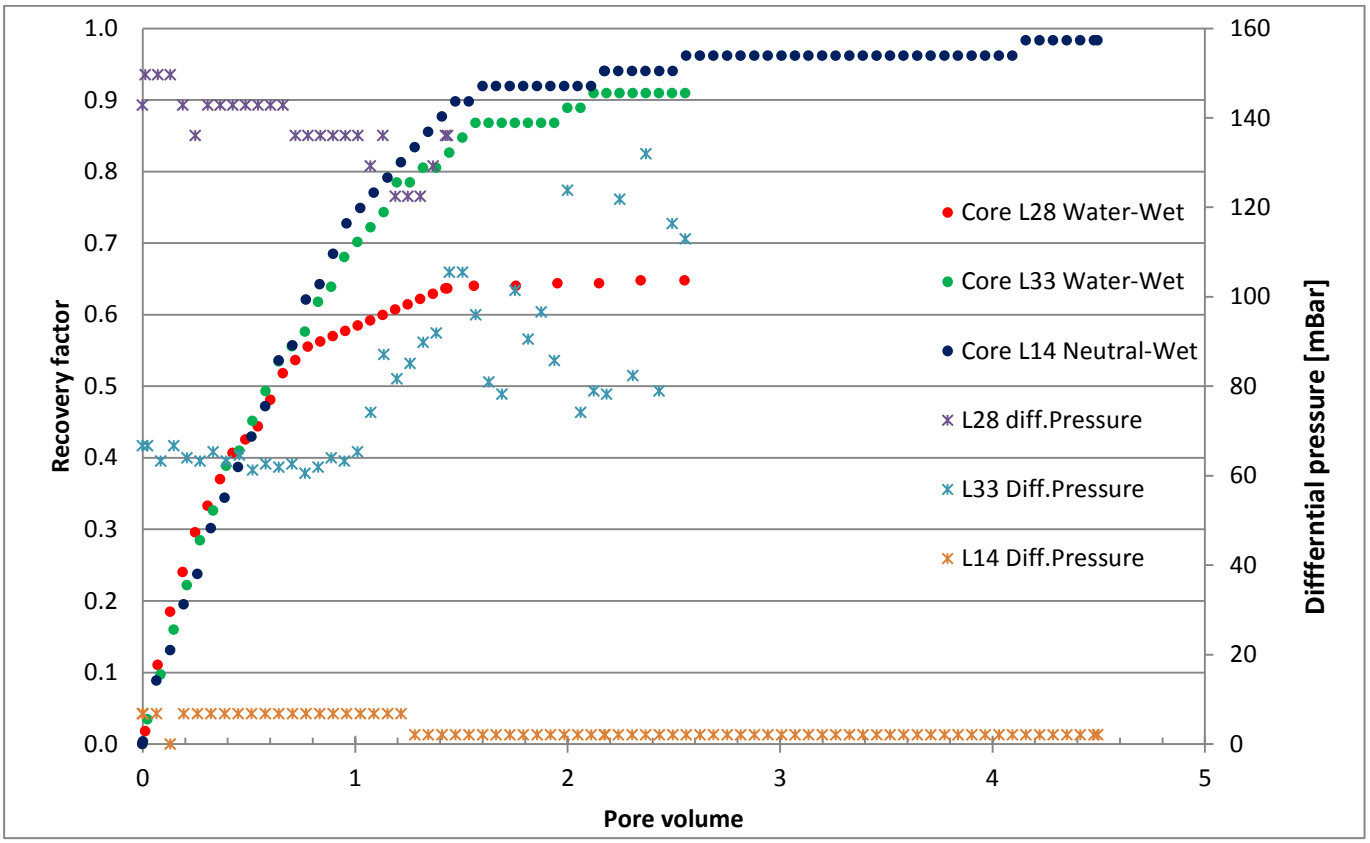

Figure 38: Recovery factor and differential pressure vs. pore volume foam injected into water-wet and neutral-wet cores. The cores are not fractured.

7.2.2 The effect of CO_2-foam injection in fractured cores

The CO_2-foam injections in fractured cores performed by Ane Skibenes and Anders Cristophersen are presented in Figure 39 and Table 8, and reached end-point oil-saturation after 5 PV for water-wet cores and after 4.5-6PV for a neutral/oil wet core. By injecting CO_2-foam into a fractured core plug, it is expected that the foam will increase the viscosity of the CO_2 and thereby increase the differential pressure which will force the injected fluid into the matrix.

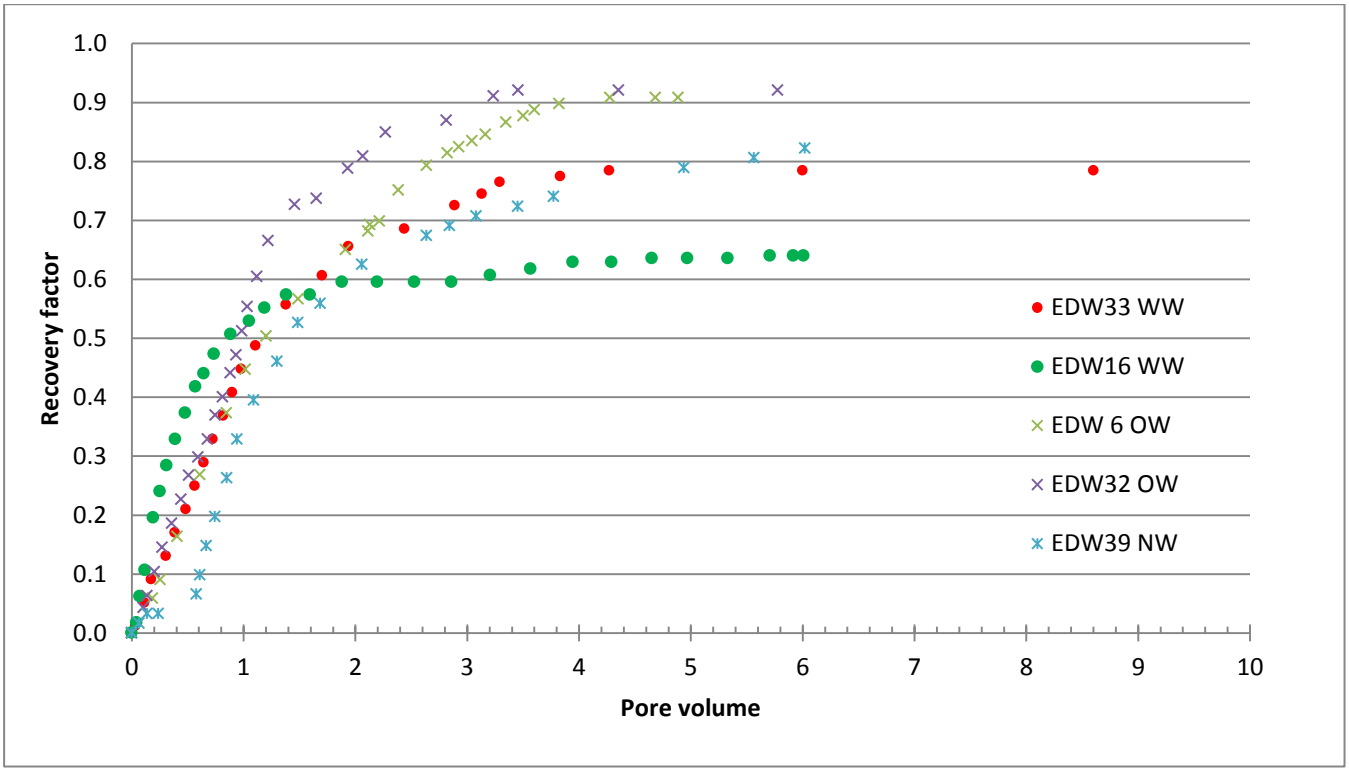

Figure 39: Recovery factor vs. pore volume foam injected into fractured water-wet and oil-wet cores. Modified from (Cristophersen, 2012)

Figure 40 shows the oil recovery and differential pressure vs. PV for CO_2-foam and CO_2 injection for whole and fractured water-wet cores. The final recovery factor is almost the same, but the rate of oil production was much higher for the CO_2-foam injection. After 1 PV injected the 30% of the oil has been recovered for CO_2-injection compared to 55% for CO_2-foam. The differential pressure for EDW16 and EDW33 varies between 50 and 250mbar, which means that foam has not been destroyed inside the core. The observed fluctuation in the differential pressure is related to the creation and destruction of lamellae. This means the CO_2-foam injection successfully managed to increase the differential pressure and thereby force the foam inside the matrix.

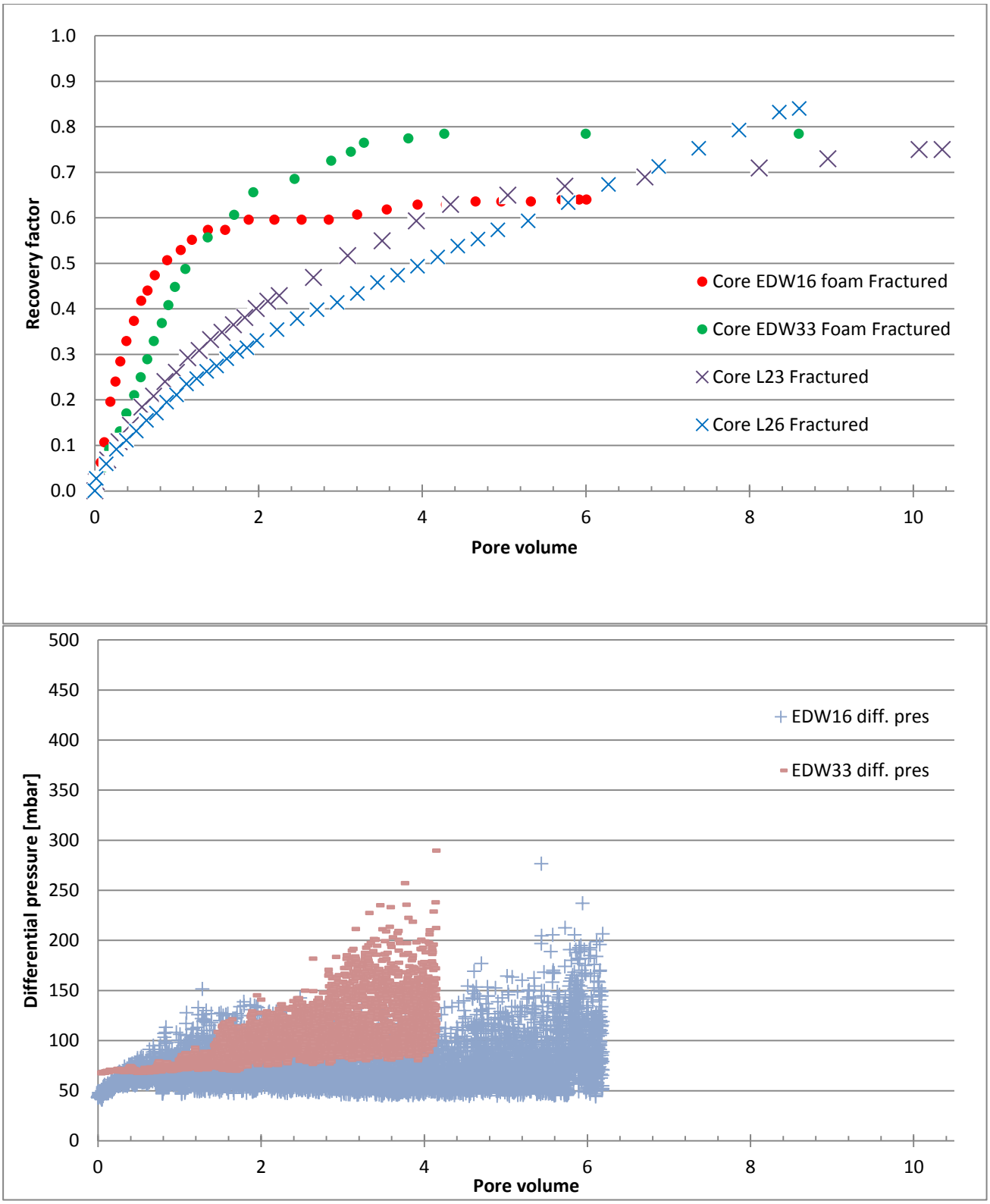

Figure 40: Recovery factor (top) and differential pressure (bottom) vs. pore volume CO_2 and CO_2-foam injected into water-wet fractured cores.

8 Conclusions

Based on the experiments presented in this thesis the following conclusions may be drawn:

The injection of CO_2 and CO_2-foam, at miscible conditions with the oil, has proven to be an efficient method for oil recovery in limestone, both in whole and fractured core plugs. Oil recovery during CO_2 injection exceeds that of water flooding because the injected fluid (CO_2) develops miscibility with the oil phase.

Contribution from diffusion with CO_2 injection was an important recovery mechanism and the rate of oil recovery per volume CO_2 injected was improved during a Huff and Puff experiment. The production rate increased after an incubation period, and led to a lower amount of pore volumes injected.

The presence of fractures reduces the rate of production during pure CO_2 injection and the recovery from the matrix is driven by diffusion of CO_2. The final recovery is less affected by the presence of fractures, but the number of pore volumes needed, using the same injection rate, is much higher for fractured cores compared to whole cores.

The presence of water in fractured cores seems to reduce the diffusion process and thereby decrease the rate of production and the final recovery.

The combined effect of wettability and on the oil recovery efficiency during CO_2 injection show that a reduced oil recovery rate for a neutral-wet core compared to water-wet core during the 2 first pore volume and may be affected by wettability and high water saturation during CO_2 injection. During CO_2 –foam injection, whole cores with the neutral wettability have a much lower differential pressure then water-wet core which could mean the foam gets destroyed inside the cores.

Secondary CO_2 –foam does not accelerate or enhance oil recovery in whole core plugs. For fractured core plugs, the rate of recovery was significantly improved during CO_2-foam injection compared with pure CO_2 injection.

9 Nomenclature

CO_2	Carbon dioxide
EOR	Enhanced oil recovery
MMP	Minimum miscibility pressure
WAG	Water alternating gas
MCM	Multiple Contact Miscibility
WAG	Water alternating
Φ_A	Absolute porosity
Φ	Effective porosity
Vp	Pore volume in matrix (except fractures)
Vb	Bulk volume of rock samples
ρ	Density of fluid
V_i	Volume of fluid, where i = o, g or w (oil, gas or water respectively)
S_i	Saturation of fluid, where i = o, g or w (oil, gas or water respectively)
S_{wi}	Irreducible water saturation
S_{or}	Irreducible oil saturation
R_f	Recovery factor from the experiment [%OOIP]
OOIP	Original Oil In place
PV	Pore volume
PV_{frac}	Pore volume after fracturing of rock material
m_d	Weight of dry rock samples
m_s	Weight of saturated rock sample
Q	Fluid flow rate
μ	Fluid viscosity
Δp	Pressure drop across the unit length
L	Sample length
A	Cross section area
K	Absolute permeability
k_r	Relative permeability
K_e	Effective permeability
λ	Mobility of a fluid
M	Mobility ratio
K_{matrix}	Absolute permeability of matrix in whole rock material
K_{frac}	Fracture permeability
I_{A-H}	Amott-Harvey index
I_w	Amott water index
I_o	Amott oil index
σ	Interfacial tension
P_c	Capillary pressure
R	Pore radius
θ	Wetting angle between two fluids
N_c	Capillary number
V_f	Viscous force
C_f	Capillary force
D_o	Diffusion coefficient in the absence of a porous media
D	Effective diffusion coefficient
C	Concentration of one component
F	Formation electrical resistivity
h^{cr}	Critical thickness
CMG	Computer Modeling Group
DP	Differential pressure
F	Formation electrical resistivity

10 References

ABDALLAH, W., J.S. BUCKLEY, A. CARNEGIE, J. EDWARDS, B. HEROLD, E. FORDHAM,, A. GRAUE, T. H., N. SELEZNEV, C. SIGNER, H. HUSSAIN, B. MONTARON, AND & ZIAUDDIN, M. 2007. Fundamentals of Wettability. *Oilfield Review. www.SLB.com, Schlumberger.*

ALVAREZ, J. M., RIVAS, H. J. & ROSSEN, W. R. 2001. Unified Model for Steady-State Foam Behavior at High and Low Foam Qualities. *SPE Journal,* 6**,** 325-333.

AMOTT, E. 1959. *Observations Relating to the Wettability of Porous Rock*.

ANDERSON, W. 1986a. Wettability Literature Survey- Part 2: Wettability Measurement. *Journal of Petroleum Technology,* 38**,** 1246-1262.

ANDERSON, W. G. 1986b. Wettability Literature Survey- Part 1: Rock/Oil/Brine Interactions and the Effects of Core Handling on Wettability. *Journal of Petroleum Technology,* 38**,** 1125-1144.

ANDERSON, W. G. 1987. Wettability Literature Survey Part 5: The Effects of Wettability on Relative Permeability. *Journal of Petroleum Technology,* 39**,** 1453-1468.

ANDRIANOV, A., FARAJZADEH, R., NICK, M. M., TALANANA, M. & ZITHA, P. L. J. 2011. Immiscible Foam for Enhancing Oil Recovery: Bulk and Porous Media Experiments. *SPE Enhanced Oil Recovery Conference.* Kuala Lumpur, Malaysia: Society of Petroleum Engineers.

ARONSON, A. S., BERGERON, V., FAGAN, M. E. & RADKE, C. J. 1994. The influence of disjoining pressure on foam stability and flow in porous media. *Colloids and Surfaces A: Physicochemical and Engineering Aspects,* 83**,** 109-120.

ASPENES, E. G., ARNE; RAMSDAL, JOHANNES 2003. In-Situ Wettability Distribution and Wetting Stability in Outcrop Chalk Aged in Crude Oil. *Journal of Petroleum Science and Engineering 2003,* 39**,** 337-350.

BAIRD, S. 2013. Master Thesis: CO2 EOR by diffusion in fractured chalk.

BIKERMAN, J. J. 1973. Foams, New York, Springer Verlag.

BROWN, R. J. S. & FATT, I. 1956. *Measurements of Fractional Wettability of Oil Fields Rocks by the Nuclear Magnetic Relaxation Method*.

CRAIG, F. F. 1971. The Reservoir Engineering Aspects of Waterflooding. *H. L. Doherty Memorial Fund of AIME.*

CRISTOPHERSEN, A. 2012. Master Thesis: Økt oljeutvinning ved injeksjon av CO2-skum i en oppsprukket karbonatbergart ved forskjellige fuktforhold.

DONALDSON, E. C. & THOMAS, R. D. 1971. Microscopic Observations of Oil Displacement in Water-Wet and Oil-Wet Systems. *Fall Meeting of the Society of Petroleum Engineers of AIME.* New Orleans, Louisiana: 1971.

EPA, U. S. E. P. A. 2012. http://www.epa.gov/climatechange/ghgemissions/gases/co2.html.

FALLS, A. H., HIRASAKI, G. J., PATZEK, T. W., GAUGLITZ, D. A., MILLER, D. D. & RATULOWSKI, T. 1988. Development of a Mechanistic Foam Simulator: The Population Balance and Generation by Snap-Off. *SPE Reservoir Engineering,* 3**,** 884-892.

FARAJZADEH, R., ANDRIANOV, A., KRASTEV, R., HIRASAKI, G. & ROSSEN, W. R. 2012. Foam-Oil Interaction in Porous Media: Implications for Foam Assisted Enhanced Oil Recovery. *SPE EOR Conference at Oil and Gas West Asia.* Muscat, Oman: Society of Petroleum Engineers.

FARAJZADEH, R., ANDRIANOV, A. & ZITHA, P. L. J. 2009. Foam Assisted Enhanced Oil Recovery at Miscible and Immiscible Conditions. *Kuwait International Petroleum Conference and Exhibition.* Kuwait City, Kuwait: Society of Petroleum Engineers.

FARAJZADEH, R., MURUGANATHAN, R., KRASTEV, R. & ROSSEN, W. R. 2010. Effect of Gas Type on Foam Film Permeability and Its Implications for Foam Flow in Porous Media. *SPE*

EUROPEC/EAGE Annual Conference and Exhibition. Barcelona, Spain: Society of Petroleum Engineers.
FRIEDMANN, F., CHEN, W. H. & GAUGLITZ, P. A. 1991. Experimental and Simulation Study of High-Temperature Foam Displacement in Porous Media. *SPE Reservoir Engineering,* 6**,** 37-45.
GAUGLITZ, P. A., FRIEDMANN, F., KAM, S. I. & ROSSEN, W. R. 2002. Foam Generation in Porous Media. *SPE/DOE Improved Oil Recovery Symposium.* Tulsa, Oklahoma: Copyright 2002, Society of Petroleum Engineers Inc.
GRAUE, A., VIKSUND, B. G. & BALDWIN, B. A. 1999. Reproducible Wettability Alteration of Low-Permeable Outcrop Chalk. *SPE Reservoir Evaluation & Engineering,* 2**,** 134-140.
HAUGEN, M. 2012. Master Thesis: CO2 Injection in Fractured Chalk for Enhanced Oil Recovery.
HIRASAKI, G. J. & LAWSON, J. B. 1985. Mechanisms of Foam Flow in Porous Media: Apparent Viscosity in Smooth Capillaries. *Society of Petroleum Engineers Journal,* 25**,** 176-190.
HOEFNER, M. L., EVANS, E. M., BUCKLES, J. J. & JONES, T. A. 1995. CO2 Foam: Results From Four Developmental Field Trials. *SPE Reservoir Engineering,* 10**,** 273-281.
HOGNESEN, E. J., STRAND, S. & AUSTAD, T. 2005. Waterflooding of Preferential Oil-Wet Carbonates: Oil Recovery Related to Reservoir Temperature and Brine Composition. *SPE Europec/EAGE Annual Conference.* Madrid, Spain: Society of Petroleum Engineers.
HONARPOUR, M. M., S.M. 1988. Relative-Permeability Measurements: An Overview. *Journal of Petroleum Technology,* 40**,** 963-966.
IEA, I. E. A. 2013. http://www.iea.org/topics/ccs/.
JIMENEZ, A. J., RADKE, C.J 1989. In Oil-field Chemistry: Enhanced Recovery and Production Stimulation.
KAM, S. I. & ROSSEN, W. R. 2002. A Model for Foam Generation in Homogeneous Media. *SPE Annual Technical Conference and Exhibition.* San Antonio, Texas: Copyright 2002, Society of Petroleum Engineers Inc.
KOVSCEK, A. R., PATZEK, T. W. & RADKE, C. J. 1993. Simulation of Foam Transport in Porous Media. *SPE Annual Technical Conference and Exhibition.* Houston, Texas: 1993 Copyright 1993, Society of Petroleum Engineers, Inc.
LAKE, L. W. 1989. *Enhanced oil recovery,* Englewood Cliffs, N.J., Prentice Hall.
LANGLO, S. 2013. CO2 and CO2-foam injection into Limestone rock for Enhanced Oil Recovery.
LIEN, J. R. 2011. *PTEK 212 Reservoarteknikk I*.
MANI, N. 2011. Master Thesis: An Experimental Study of Foam Injection for Enhanced Oil Recovery in Carbonate Rocks.
MORROW, N. R. B., J 2006. Wettability and Oil Recovery by Imbibition and Viscous Displacement from Fractured and Heterogeneous Carbonates. 57-62.
NETL, N. E. T. L. 2010. Carbon Dioxide Enhanced Oil Recovery - Untapped Domestic Energy Supply and Long Term Carbon Storage Solution.
NIST 2012. Thermophysical Properties of Fluid Systems http://webbook.nist.gov/cgi/chemistry/fluid/.
NOBAKHT, M., MOGHADAM, S. & GU, Y. 2008. Mutual interactions between crude oil and CO2 under different pressures. *Fluid Phase Equilibria,* 265**,** 94-103.
NONNEKES, L. E., COS, S. & ROSSEN, W. R. 2012. Effect of Gas Diffusion on Mobility of Foam for EOR. *SPE Annual Technical Conference and Exhibition.* San Antonio, Texas, USA: Society of Petroleum Engineers.
OLDENBURG, C. M. P., K ; BENSON S.M. 2000. Process Modeling of CO2 Injection into Natual Gas Reservoirs for Carbon Sequestration and Enhanced Gas Recovery. 293-298.
RANSOHOFF, T. C. & RADKE, C. J. 1988. Mechanisms of Foam Generation in Glass-Bead Packs. *SPE Reservoir Engineering,* 3**,** 573-585.

RAZA, S. H., TREIBER, L. E. & ARCHER, D. L. 1968. Wettability of reservoir rocks and its evaluation. 32:4**,** 2-4, 6-7.
ROSSEN, W. R. 1996. Foams in Enhanced Oil Recovery, in Foams: Theory Measurement and Application.
SAADAWI, H. N. H., JOHNS, A. & WALTER, K. 2011. A Study to Evaluate the Impact of CO2-EOR on Existing Oil Field Facilities. *SPE Project and Facilities Challenges Conference at METS.* Doha, Qatar: Society of Petroleum Engineers.
SALATHIEL, R. A. 1973. Oil Recovery by Surface Film Drainage In Mixed-Wettability Rocks. *Journal of Petroleum Technology,* 25**,** 1216-1224.
SANCHEZ, J. M. & HAZLETT, R. D. 1992. Foam Flow Through an Oil-Wet Porous Medium: A Laboratory Study. *SPE Reservoir Engineering,* 7**,** 91-97.
SCHECHTER, D. S., GRIGG, R., GUO, B. & SCHNEIDER, B. 1998. Wellman Unit CO2 Flood: Reservoir Pressure Reduction and Flooding the Water/Oil Transition Zone. *SPE Annual Technical Conference and Exhibition.* New Orleans, Louisiana: Society of Petroleum Engineers.
SCIENCEDIRECT 2011. Development of CO2 liquefaction cycles for CO2 sequestration. http://www.sciencedirect.com/science/article/pii/S1359431111005114?np=y.
SCRIPPS INSTITUTION OF OCEANOGRAPHY, U. S. D. 2013. http://keelingcurve.ucsd.edu/.
SKARSTAD, M., SKAUGE, A. 2011. Reservoarteknikk II, PTEK 213.
SKAUGE, A., AARRA, M. G., SURGUCHEV, L., MARTINSEN, H. A. & RASMUSSEN, L. 2002. Foam-Assisted WAG: Experience from the Snorre Field. *SPE/DOE Improved Oil Recovery Symposium.* Tulsa, Oklahoma: Copyright 2002, Society of Petroleum Engineers Inc.
SRIVASTAVA, M. & NGUYEN, Q. P. 2010. Application of Gas for Mobility Control in Chemical EOR in Problematic Carbonate Reservoirs. *SPE Improved Oil Recovery Symposium.* Tulsa, Oklahoma, USA: Society of Petroleum Engineers.
STEVENS, J. E., HARPOLE, K. J., ZORNES, D. R. & MARTIN, F. D. 1992. CO2 Foam Field Verification Pilot Test at EVGSAU: Phase II - Foam Injection Design and Operating Plan. *SPE Annual Technical Conference and Exhibition.* Washington, D.C.: 1992 Copyright 1992, Society of Petroleum Engineers Inc.
SVENNINGSEN, S. 2011. Master Thesis: An experimental study of CO2 injection for enhanced oil recovery in chalk and limestone.
THOMAS, C. P. 2001. Methane Hydrates: Major Energy Source for the Future or Wishful Thinking? *SPE Annual Technical Conference and Exhibition.* New Orleans, Louisiana: Copyright 2001, Society of Petroleum Engineers Inc.
TURTA, A. T. & SINGHAL, A. K. 2002. Field Foam Applications in Enhanced Oil Recovery Projects: Screening and Design Aspects. *Journal of Canadian Petroleum Technology,* 41.
ZOLOTUKHIN, A. B., URSIN, J.R. 2000. *Introduction to Petroleum Reservoir Engineering*, HøyskoleForlaget.

11 Appendix A : Data- file from CMG-simulation

```
INUNIT SI
WSRF WELL 1
WSRF GRID TIME
OUTSRF GRID SO SG SW PRES *X 'NC10' *X 'CO2'
OUTSRF RES NONE
WPRN GRID 0
OUTPRN GRID NONE
OUTPRN RES NONE
** WPRN ITER MATRIX

**$  Distance units: m
RESULTS XOFFSET         0.0000
RESULTS YOFFSET         0.0000
RESULTS ROTATION        0.0000  **$  (DEGREES)
RESULTS AXES-DIRECTIONS 1.0 -1.0 1.0
**$ *************************************************************************
**$ Definition of fundamental cartesian grid
**$ *************************************************************************
GRID VARI 34 21 1
KDIR DOWN
DI IVAR
 0.1 32*0.002229 0.1
DJ JVAR
 20*0.00249 0.05
DK ALL
 714*0.01031067

**$ Property: NULL Blocks  Max: 1  Min: 1
**$  0 = null block, 1 = active block
NULL CON          1

**$ Property: Porosity  Max: 0.254  Min: 0.254
POR ALL
0.999 32*0.223  0.999
0.999 32*0.223  0.999
0.999 32*0.223  0.999
0.999 32*0.223  0.999
0.999 32*0.223  0.999
0.999 32*0.223  0.999
0.999 32*0.223  0.999
0.999 32*0.223  0.999
0.999 32*0.223  0.999
0.999 32*0.223  0.999
0.999 32*0.223  0.999
0.999 32*0.223  0.999
0.999 32*0.223  0.999
0.999 32*0.223  0.999
0.999 32*0.223  0.999
0.999 32*0.223  0.999
0.999 32*0.223  0.999
0.999 32*0.223  0.999
0.999 32*0.223  0.999
0.999 32*0.223  0.999
0.999 32*0.223  0.999
34*0.999

**$ Property: Permeability I (md)   Max: 58.639  Min: 58.639
PERMI ALL
500000   32*58.639    500000
500000   32*58.639    500000
500000   32*58.639    500000
500000   32*58.639    500000
```

500000 32*58.639 500000
500000 32*58.639 500000
500000 32*58.639 500000
500000 32*58.639 500000
500000 32*58.639 500000
500000 32*58.639 500000
500000 32*58.639 500000
500000 32*58.639 500000
500000 32*58.639 500000
500000 32*58.639 500000
500000 32*58.639 500000
500000 32*58.639 500000
500000 32*58.639 500000
500000 32*58.639 500000
500000 32*58.639 500000
34*500000

**$ Property: Permeability J (md) Max: 58.639 Min: 58.639
PERMJ ALL
500000 32*58.639 500000
500000 32*58.639 500000
500000 32*58.639 500000
500000 32*58.639 500000
500000 32*58.639 500000
500000 32*58.639 500000
500000 32*58.639 500000
500000 32*58.639 500000
500000 32*58.639 500000
500000 32*58.639 500000
500000 32*58.639 500000
500000 32*58.639 500000
500000 32*58.639 500000
500000 32*58.639 500000
500000 32*58.639 500000
500000 32*58.639 500000
500000 32*58.639 500000
500000 32*58.639 500000
500000 32*58.639 500000
500000 32*58.639 500000
34*500000
**$ Property: Permeability K (md) Max: 58.639 Min: 58.639
PERMK ALL
500000 32*58.639 500000
500000 32*58.639 500000
500000 32*58.639 500000
500000 32*58.639 500000
500000 32*58.639 500000
500000 32*58.639 500000
500000 32*58.639 500000
500000 32*58.639 500000
500000 32*58.639 500000
500000 32*58.639 500000
500000 32*58.639 500000
500000 32*58.639 500000
500000 32*58.639 500000
500000 32*58.639 500000
500000 32*58.639 500000
500000 32*58.639 500000
500000 32*58.639 500000
500000 32*58.639 500000
500000 32*58.639 500000
500000 32*58.639 500000
500000 32*58.639 500000
500000 32*58.639 500000
500000 32*58.639 500000
34*500000

**$ Property: Pinchout Array Max: 1 Min: 1
**$ 0 = pinched block, 1 = active block

```
PINCHOUTARRAY CON          1
SECTORARRAY 'FRACTURE1'  ALL
 1 33*0 1 33*0 1 33*0 1 33*0 1 33*0 1 33*0 1 33*0 1 33*0 1 33*0 1 33*0 1 33*0 1
 33*0 1 33*0 1 33*0 1 33*0 1 33*0 1 33*0 1 33*0 1 33*0 1 33*0 1 33*0 1 33*0 1 33*0
SECTORARRAY 'FRACTURE2'  ALL
 33*0 1 33*0 1 33*0 1 33*0 1 33*0 1 33*0 1 33*0 1 33*0 1 33*0 1 33*0 1 33*0 1 33*0
 1 33*0 1 33*0 1 33*0 1 33*0 1 33*0 1 33*0 1 33*0 1 33*0 1 33*0 1 33*0 1 33*0 1*1
SECTORARRAY 'FRACTURE3'  ALL
 681*0 32*1 1*0
SECTORARRAY 'MATRIX'  ALL
 0 32*1 2*0 32*1 2*0 32*1 2*0 32*1 2*0 32*1 2*0 32*1 2*0 32*1 2*0 32*1 2*0 32*1 2*0
 32*1 2*0 32*1 2*0 32*1 2*0 32*1 2*0 32*1 2*0 32*1 2*0 32*1 2*0 32*1 2*0 32*1 2*0
 32*1 2*0 32*1 2*0 32*1 2*0 32*1 35*0

**DEPTH 1 34 1 1000

DEPTH-TOP ALL
714*1000
**$ Model and number of components

MODEL PR
**=-=-=Component Selection/Properties
**REM
NC 2 2
COMPNAME 'CO2' 'NC10'
HCFLAG
0 1
VISCOR HZYT
MIXVC 1
VISCOEFF 0.1023 0.023364 0.058533 -0.040758 0.0093324
PVC3 1.2
MW
44.01 142.286
AC
0.225 0.49
PCRIT
72.8 20.8
VCRIT
0.094 0.603
TCRIT
304.2 617.6
PCHOR
78 433.5
SG
0.818 0.734
TB
-78.45 174.15
OMEGA
0.457236 0.457236
OMEGB
0.0777961 0.0777961
VSHIFT
0 0
HEATING_VALUES
0 6473.36
VISVC
0.094 0.603
BIN
0.11

TRES 20
VISW 1.09

**DIFCOR-OIL          *WILKE
*DIFFC-OIL            0.0001 0
```

```
ROCKFLUID
RPT 1
**$      Sw      krw      krow      Pcow
SWT
        0       0      1.0        0
      1.0      1.0        0        0
**$      Sl      krg      krog
SLT
        0       1        0
        1       0        1
RPT 2
**$      Sw      krw      krow         Pcow
SWT
     0.13       0        1   21.75568367
     0.15   0.0014   0.9846   17.40454694
     0.18   0.0036   0.9539   12.32822075
     0.23   0.0074   0.8881   7.977084013
      0.3   0.0127   0.7655   4.786250408
     0.33    0.015   0.7021   3.843504115
    0.391   0.0196    0.553   2.921730302
    0.469   0.0581   0.3229   2.707813916
    0.564   0.1312   0.1444   2.444918235
    0.632   0.2036   0.0408   2.270423148
    0.674   0.2574   0.0058   2.152362305
    0.702   0.2974   0.0003   2.069748722
     0.71   0.3095   0.0002   2.047354871
    0.718   0.3218   0.0001   2.026454911
    0.722   0.3281        0  -2.175568367
**$      Sl      krg      krog
SLT
        0.13       1        0
        1       0        1


RTYPE ALL
1*1  32*2  1*1
1*1  32*2  1*1
1*1  32*2  1*1
1*1  32*2  1*1
1*1  32*2  1*1
1*1  32*2  1*1
1*1  32*2  1*1
1*1  32*2  1*1
1*1  32*2  1*1
1*1  32*2  1*1
1*1  32*2  1*1
1*1  32*2  1*1
1*1  32*2  1*1
1*1  32*2  1*1
1*1  32*2  1*1
1*1  32*2  1*1
1*1  32*2  1*1
1*1  32*2  1*1
1*1  32*2  1*1
1*1  32*2  1*1
1*1  32*2  1*1
34*1


INITIAL

USER_INPUT



**VERTICAL BLOCK_CENTER WATER_OIL
**REFPRES
```

```
**9200
**REFDEPTH
**1000
**DWOC
**5000

**REFPRES
**9200

**REFDEPTH
**1000

**DWOC
**5000

*PRES    *KVAR  9200.0
*SW      *IJK                        1 1:21 1    0
                                                                    34 1:21 1    0
                                                                    2:33 21 1    0
                                                                    2:33 1:20 1  0.13
ZGLOBALC 'NC10' ALL
 0 32*1 2*0 32*1 2*0 32*1 2*0 32*1 2*0 32*1 2*0 32*1 2*0 32*1 2*0 32*1 2*0 32*1
 2*0 32*1 2*0 32*1 2*0 32*1 2*0 32*1 2*0 32*1 2*0 32*1 2*0 32*1 2*0 32*1 2*0
 32*1 2*0 32*1 2*0 32*1 2*0 32*1 2*0 32*1 2*0 32*1 35*0
ZGLOBALC 'CO2' ALL
 1 32*0 2*1 32*0 2*1 32*0 2*1 32*0 2*1 32*0 2*1 32*0 2*1 32*0 2*1 32*0 2*1 32*0
 2*1 32*0 2*1 32*0 2*1 32*0 2*1 32*0 2*1 32*0 2*1 32*0 2*1 32*0 2*1 32*0 2*1
 32*0 2*1 32*0 2*1 32*0 2*1 32*0 2*1 32*0 2*1 32*0 35*1


NUMERICAL
MAXSTEPS 150000
DTMAX 0.001
DTMIN 0.00001
NORM PRESS 200
NORM SATUR 0.6
NORM GMOLAR 0.3
NORM AQUEOUS 0.6
NORM TEMP 10
MAXCHANGE GMOLAR 0.9
CONVERGE HC 0.02
NCHECK-CEQ 3
NEWTONCYC 100
ITERMAX 200
ITERMIN 100
RUN

DATE 2013 4 11
DTWELL 0.0001


REFINE 1 3 1
RANGE 9:26 15:20 1

REFINE 3 3 1
RANGE 2:8 15:20 1
RANGE 27:33 15:20 1

REFINE 3 1 1
RANGE 2:8 1:14 1
RANGE 27:33 1:14 1

DATE 2013 4 11.0014
DATE 2013 4 11.08333
DATE 2013 4 11.12500
DATE 2013 4 11.16667
DATE 2013 4 11.20833
```

```
DTWELL 0.0001
DATE 2013 4 11.25000
DATE 2013 4 11.29167
DATE 2013 4 11.33333
DATE 2013 4 11.37500
DATE 2013 4 11.41667
DATE 2013 4 11.45833
DATE 2013 4 11.50000
DATE 2013 4 11.54167
DATE 2013 4 11.58333
DATE 2013 4 11.62500
DATE 2013 4 11.66667
DATE 2013 4 11.70833
DATE 2013 4 11.75000
DATE 2013 4 11.79167
DATE 2013 4 11.83333
DATE 2013 4 11.87500
DATE 2013 4 11.91667
DATE 2013 4 11.95833
DATE 2013 4 12.00000
DATE 2013 4 12.04167
DATE 2013 4 12.08333
DATE 2013 4 12.12500
DATE 2013 4 12.16667
DATE 2013 4 12.20833
DATE 2013 4 12.25000
DATE 2013 4 12.29167
DATE 2013 4 12.33333
DATE 2013 4 12.37500
DATE 2013 4 12.41667
DATE 2013 4 12.45833
DATE 2013 4 12.50000
DATE 2013 4 12.54167
DATE 2013 4 12.58333
DATE 2013 4 12.62500
DATE 2013 4 12.66667
DATE 2013 4 12.70833
DATE 2013 4 12.75000
DATE 2013 4 12.79167
DATE 2013 4 12.83333
DATE 2013 4 12.87500
DATE 2013 4 12.91667
DATE 2013 4 12.95833
DATE 2013 4 13.00000

RESULTS SPEC 'Permeability I'
RESULTS SPEC SPECNOTCALCVAL -99999
RESULTS SPEC REGION 'All Layers (Whole Grid)'
RESULTS SPEC REGIONTYPE 'REGION_WHOLEGRID'
RESULTS SPEC LAYERNUMB 0
RESULTS SPEC PORTYPE 1
RESULTS SPEC CON 51.045
RESULTS SPEC SPECKEEPMOD 'YES'
RESULTS SPEC STOP


RESULTS SPEC 'Permeability J'
RESULTS SPEC SPECNOTCALCVAL -99999
RESULTS SPEC REGION 'All Layers (Whole Grid)'
RESULTS SPEC REGIONTYPE 'REGION_WHOLEGRID'
RESULTS SPEC LAYERNUMB 0
RESULTS SPEC PORTYPE 1
RESULTS SPEC CON 51.045
RESULTS SPEC SPECKEEPMOD 'YES'
RESULTS SPEC STOP
```

```
RESULTS SPEC 'Permeability K'
RESULTS SPEC SPECNOTCALCVAL -99999
RESULTS SPEC REGION 'All Layers (Whole Grid)'
RESULTS SPEC REGIONTYPE 'REGION_WHOLEGRID'
RESULTS SPEC LAYERNUMB 0
RESULTS SPEC PORTYPE 1
RESULTS SPEC CON 51.045
RESULTS SPEC SPECKEEPMOD 'YES'
RESULTS SPEC STOP

RESULTS SPEC 'Porosity'
RESULTS SPEC SPECNOTCALCVAL -99999
RESULTS SPEC REGION 'All Layers (Whole Grid)'
RESULTS SPEC REGIONTYPE 'REGION_WHOLEGRID'
RESULTS SPEC LAYERNUMB 0
RESULTS SPEC PORTYPE 1
RESULTS SPEC CON 0.254
RESULTS SPEC SPECKEEPMOD 'YES'
RESULTS SPEC STOP

RESULTS SPEC 'Pressure'
RESULTS SPEC SPECNOTCALCVAL -99999
RESULTS SPEC REGION 'All Layers (Whole Grid)'
RESULTS SPEC REGIONTYPE 'REGION_WHOLEGRID'
RESULTS SPEC LAYERNUMB 0
RESULTS SPEC PORTYPE 1
RESULTS SPEC CON 9230
RESULTS SPEC SPECKEEPMOD 'YES'
RESULTS SPEC STOP

RESULTS SPEC 'Rock Density'
RESULTS SPEC SPECNOTCALCVAL -99999
RESULTS SPEC REGION 'All Layers (Whole Grid)'
RESULTS SPEC REGIONTYPE 'REGION_WHOLEGRID'
RESULTS SPEC LAYERNUMB 0
RESULTS SPEC PORTYPE 1
RESULTS SPEC CON 2012
RESULTS SPEC SPECKEEPMOD 'YES'
RESULTS SPEC STOP

RESULTS SPEC 'Water Saturation'
RESULTS SPEC SPECNOTCALCVAL -99999
RESULTS SPEC REGION 'All Layers (Whole Grid)'
RESULTS SPEC REGIONTYPE 'REGION_WHOLEGRID'
RESULTS SPEC LAYERNUMB 0
RESULTS SPEC PORTYPE 1
RESULTS SPEC CON 0
RESULTS SPEC SPECKEEPMOD 'YES'
RESULTS SPEC STOP

RESULTS SPEC 'Initial Water Saturation'
RESULTS SPEC SPECNOTCALCVAL -99999
RESULTS SPEC REGION 'All Layers (Whole Grid)'
RESULTS SPEC REGIONTYPE 'REGION_WHOLEGRID'
RESULTS SPEC LAYERNUMB 0
RESULTS SPEC PORTYPE 1
RESULTS SPEC CON 0
RESULTS SPEC SPECKEEPMOD 'YES'
RESULTS SPEC STOP

RESULTS SPEC 'Block Temperature'
```

```
RESULTS SPEC SPECNOTCALCVAL -99999
RESULTS SPEC REGION 'All Layers (Whole Grid)'
RESULTS SPEC REGIONTYPE 'REGION_WHOLEGRID'
RESULTS SPEC LAYERNUMB 0
RESULTS SPEC PORTYPE 1
RESULTS SPEC CON 20
RESULTS SPEC SPECKEEPMOD 'YES'
RESULTS SPEC STOP


RESULTS SPEC 'Global Composition$C' 'CO2'
RESULTS SPEC SPECNOTCALCVAL -99999
RESULTS SPEC REGION 'All Layers (Whole Grid)'
RESULTS SPEC REGIONTYPE 'REGION_WHOLEGRID'
RESULTS SPEC LAYERNUMB 0
RESULTS SPEC PORTYPE 1
RESULTS SPEC CON 1
RESULTS SPEC SPECKEEPMOD 'YES'
RESULTS SPEC STOP


RESULTS SPEC 'Global Composition$C' 'NC10'
RESULTS SPEC SPECNOTCALCVAL -99999
RESULTS SPEC REGION 'All Layers (Whole Grid)'
RESULTS SPEC REGIONTYPE 'REGION_WHOLEGRID'
RESULTS SPEC LAYERNUMB 0
RESULTS SPEC PORTYPE 1
RESULTS SPEC CON 2
RESULTS SPEC SPECKEEPMOD 'YES'
RESULTS SPEC STOP


RESULTS SPEC 'Grid Thickness'
RESULTS SPEC SPECNOTCALCVAL -99999
RESULTS SPEC REGION 'All Layers (Whole Grid)'
RESULTS SPEC REGIONTYPE 'REGION_WHOLEGRID'
RESULTS SPEC LAYERNUMB 0
RESULTS SPEC PORTYPE 1
RESULTS SPEC CON 0.0103107
RESULTS SPEC SPECKEEPMOD 'YES'
RESULTS SPEC STOP
```